https://doi.org/10.5194/egusphere-2026-5324
Preprint. Discussion started: 9 September 2026

The influence of the Madden-Julian Oscillation and extratropical Rossby wave dynamics on daily to multi-day precipitation variability in the arid Middle East during the wet season

Andries-Jan de Vries[1], Steven B. Feldstein[2], Georgios Fragkoulidis[3], Priyanka Yadav[4,5], Daniela I.V. Domeisen[1]

[1]Institute of Earth Surface Dynamics, University of Lausanne, Lausanne, Switzerland
[2]Department of Meteorology and Atmospheric Science, The Pennsylvania State University, University Park, PA, USA
[3]Institute of Environmental Research and Sustainable Development, National Observatory of Athens, Athens, Greece
[4]Earth System Science Interdisciplinary Center (ESSIC), University of Maryland, College Park, MD, USA
[5]Global Modeling and Assimilation Office, NASA Goddard Space Flight Center, Greenbelt, MD, USA

Correspondence to: Andries-Jan de Vries (andries-jan.devries@unil.ch)

Abstract. Most of the annual precipitation in the arid Middle East falls on only a few days per year during the cool season, having important implications for water resources and hydrometeorological hazards. Previous studies have shown that daily precipitation in the Middle East is modulated by both intraseasonal variability in tropical convection related to the Madden-Julian Oscillation (MJO) and midlatitude Rossby wave dynamics. However, their respective contributions to precipitation variability and their underlying mechanisms remain largely unexplored. This study quantifies the separate and joint influence of the MJO and midlatitude Rossby wave dynamics on daily to multi-day precipitation variability in the arid Middle East during the wet season (November-April) and explores the underlying mechanisms. To this end, we use daily precipitation observations and atmospheric reanalysis data for the period 1979-2020 along with diagnostics of Rossby wave packets and Rossby wave breaking. Our findings indicate that the remote influence of the MJO and local midlatitude Rossby wave forcing operate largely independent of each other and exert an approximately equal influence on Middle Eastern precipitation variability. Consistent with previous studies, reduced (enhanced) tropical convection over the eastern Indian Ocean and Maritime Continent during MJO phases 8 and 1 (4 and 5) increases (decreases) precipitation by more than 50%. MJO convective activity influences Middle Eastern precipitation through a baroclinic response in the regional tropical circulation, consistent with the Matsuno-Gill model, inducing anomalies in the upper- and lower-tropospheric circulation, in atmospheric moisture transport into the region, and in large-scale vertical motion over the region. The immediate influence of the MJO via the regional tropical circulation does not alter the propagation and breaking of Rossby waves into the region in a manner that is consistent with wet or dry conditions. However, our findings suggest an extratropical pathway through which the MJO modulates precipitation over the Middle East with an approximately two-week lag, extending wet or dry conditions induced by the immediate MJO influence. The concurrence of the MJO with anomalous Rossby wave forcing can amplify or mute the precipitation response that would be expected from midlatitude forcing alone through strengthening or weakening the

https://doi.org/10.5194/egusphere-2026-5324
Preprint. Discussion started: 9 September 2026

atmospheric moisture supply and through reinforcing or offsetting large-scale vertical motion over the region. This study contributes to improved process understanding of tropical and extratropical controls on precipitation variability in the water-scarce Middle East with implications for medium-range to sub-seasonal prediction of precipitation and early warnings for drought and flood hazards.

1. Introduction

Precipitation in the arid Middle East has important societal implications as it can replenish scarce water resources but also gives rise to flood hazards. Much of the region's annual precipitation comes as heavy rainfall limited to only a few days per year (Almazroui and Saeed, 2020; Zittis et al., 2021). These sparse precipitation events provide an essential recharge of freshwater resources through refill of aquifers and the harvest of flood water (Abbas et al., 2020; Sherif et al., 2023; Raoufi and Tsubaki, 2025). Given that 70% of the region's agriculture is rain-fed, a prolonged absence of precipitation can result in drought with detrimental impacts on food security and the local economy (Waha et al., 2017). While water demand continuously increases due to the rapidly growing population (ESCWA, 2025), water availability is projected to decrease owing to a decline in precipitation and a rise in atmospheric evaporative demand due to climate change (Chenoweth et al., 2011; Barlow et al., 2016; Zittis et al., 2022). At the same time, infrequent precipitation at high intensity can lead to sudden flash floods in dry riverbeds or valleys known as wadis. Such flood events repeatedly cause large numbers of fatalities and widespread damage to infrastructure and property (Hochmann et al., 2022; Coleman et al., 2026). For these reasons, it is of high importance to understand the atmospheric processes that modulate precipitation variability on daily to multi-day timescales. This knowledge can support the interpretation of medium-range to sub-seasonal prediction and guide early warnings for drought and flood hazards.

Geographically, the Middle East lies at the crossroads of the European, African, and Asian continents. Accordingly, the Middle Eastern climate is influenced by circulation regimes extending from these three continents, including the midlatitude westerlies and extratropical weather systems over Europe, tropical easterlies over equatorial Africa, and the Asian monsoon. During the warm season, from June to September, the Middle East remains virtually dry due to the influence of the South Asian summer monsoon imposing large-scale subsidence over the region, inhibiting upward motion and precipitation (Tyrlis et al., 2013). Although the weather during the extended cool season is usually dry as well, extratropical weather systems, sometimes referred to as westerly disturbances or Cyprus Lows, can bring abundant precipitation (Saaroni et al., 2010; Cannon et al., 2017; Hunt et al., 2018). These midlatitude weather systems can also interact with the tropical circulation, fostering the intrusion of warm, moist air masses of tropical origin into the arid Middle East, which in turn supports the formation of deep moist convection and heavy rainstorms. Such tropical-extratropical interactions can take the form of distinct regional weather phenomena, such as the active Red Sea Trough or tropical plumes (Kahana et al., 2002; Rubin et al., 2007; De Vries et al., 2013; Tubi et al., 2017; Armon et al., 2018). In this study, the focus is on the larger-scale tropical and extratropical forcing mechanisms that shape precipitation variability and local atmospheric conditions over the Middle East. In this context, two processes are of specific interest: intraseasonal variability of tropical convection and midlatitude Rossby wave dynamics.

Intraseasonal variability in global weather and climate is dominated by the Madden-Julian Oscillation (MJO), which is characterized by anomalous tropical convection moving eastward over the tropical Indo-Pacific Oceans with a periodicity of approximately 30-60 days (Madden and Julian, 1971; Zhang et al., 2013). Previous studies have shown that intraseasonal variability in tropical convection, related to the MJO, also modulates precipitation variability across the Middle East and Southwest Asia (Hoell et al., 2012, 2013b). Stations in Saudi Arabia, Iran, and Afghanistan tend to measure increased (decreased) precipitation associated with reduced (enhanced) convection over the eastern Indian Ocean and Maritime Continent (Barlow et al., 2005; Nazemosadat and Ghaedamini, 2010; Almazroui, 2023). When expressed by the commonly used 8 MJO phases of Wheeler and Hendon (2004), existing studies have reported similar patterns with precipitation increases for MJO phases 1, 2, 7, and 8 and precipitation decreases for MJO phases 3, 4, 5, and 6 (Tippett et al., 2015; Pourasghar et al., 2015; Nazemodadat and Shahgholian, 2017; Almazroui, 2023). Other work linked MJO phases 6-8 to wet conditions and MJO phases 2-4 to dry conditions over the Middle East and Southwest Asia (Hoell et al., 2018). The profound influence of the MJO on Middle East hydrometeorological conditions is not only evident from anomalies in precipitation amounts and extreme precipitation occurrences, but also from its association with major flood events (Barlow et al., 2005; Hoell et al., 2012) and its ability to overwhelm precipitation variability at seasonal to interannual timescales (Barlow et al., 2005), sometimes unexpectedly overriding seasonal predictions (Hoell et al., 2025).

Previous studies have examined the atmospheric mechanisms through which the MJO modulates precipitation variability in the Middle East. Enhanced tropical convection over the eastern Indian Ocean and Maritime Continent induces a Rossby wave response in the form of an upper-tropospheric anticyclonic circulation and warm structure anomaly extending northwestward across South Asia and the Middle East (Barlow et al., 2005). Given that the prevailing upper-tropospheric winds are westerlies, these conditions imply cold air advection which is thermodynamically balanced by subsidence (Barlow et al., 2007; Hoell et al., 2012). In the lower troposphere, an opposite cyclonic circulation anomaly manifests with anomalous northeasterly winds over the Middle East, weakening the southwesterly atmospheric moisture transport into the region (Nazemosadat and Ghaedamini, 2010; Hoell et al., 2018). These conditions lead to a substantial precipitation decrease across the region. Conversely, for reduced tropical convective activity over the eastern Indian Ocean and Maritime Content, a reversed circulation response emerges. A cyclonic circulation anomaly establishes in the upper troposphere and an anticyclonic anomaly in the lower troposphere, associated with thermodynamically-driven ascent and strengthened moisture transport from the southwest into the Middle East (Nazemosadat and Ghaedamini, 2010; Hoell et al., 2018). This baroclinic response to tropical convection anomalies can be explained by the Matsuno-Gill model which is based on linearized wave equations in a shallow water model on an equatorial beta plane (Matsuno, 1966; Gill, 1980). However, a potential influence of the MJO on Middle Eastern precipitation variability through modulating midlatitude weather systems, which are of key importance for precipitation

https://doi.org/10.5194/egusphere-2026-5324
Preprint. Discussion started: 9 September 2026

generation at daily timescales, has not yet been investigated. Such a potential influence could arise from a regionally altered background flow over the Middle East, favoring or hindering midlatitude storms passing through the region, or via an eastward propagating Rossby wave response in the extratropical circulation modulating synoptic-scale weather systems throughout much of the Northern Hemisphere (Mundhenk et al., 2016; Guo et al., 2017; Quinting et al., 2024; Toride et al., 2026).

Midlatitude forcing has also widely been linked to precipitation formation in the Middle East. This forcing can take the form of various extratropical weather systems such as surface cyclones (e.g., the Cyprus Low), mid-tropospheric troughs and cutoff lows, and warm conveyor belts (Evans and Smith, 2006; Kumar et al., 2015; Almazroui et al., 2016; De Vries et al., 2016; Nelli et al., 2021; Breeden et al., 2023). It can be argued that these midlatitude weather systems have a common origin in extratropical Rossby waves propagating across the Middle East, often followed by the breaking of these waves into low latitudes (Vries et al., 2018; Tuel et al., 2022; Sandler et al., 2024; Francis et al., 2025). These Rossby waves originate from the North Atlantic or the North American continent several days prior to the occurrence of precipitation in the Middle East, followed by their propagation and decay over South Asia and the West Pacific (Feldstein and Dayan, 2008). Previous studies have inferred these eastward moving Rossby wave trains from EOF analysis of meridional wind fields, reflecting circumglobal wave trains, as well as from composites of upper-tropospheric meridional winds, stream function, geopotential height, or wave activity flux (Feldstein and Dayan, 2008; Saeed and Almazroui, 2019; Atif et al., 2020; Alizadeh et al., 2020; Govardhan et al., 2025). In this study, we extend previous work by explicitly identifying Rossby wave dynamics using diagnostics of Rossby wave packets and Rossby wave breaking to quantify the space-time characteristics of these processes in relation to precipitation variability over the Middle East.

Extratropical Rossby waves are not only associated with precipitation formation in the Middle East but also with anomalously dry conditions in the region. Previous studies have linked dry spells or dry extremes to different atmospheric configurations, including an expansion of the subtropical anticyclone over the Mediterranean, a ridge over the eastern Mediterranean as part of a Rossby wave, and a trough to the northeast of the region (Saaroni et al., 2015). These circulation patterns can contribute to dry conditions through subsidence, dry air advection, and surface radiative processes (Berkovic and Raveh-Rubin, 2022). These atmospheric configurations have also been linked to a decrease in Cyprus Low activity and a northward displacement of the storm track over the Mediterranean basin (Saaroni et al., 2019; Sandler et al., 2024). Existing research on the atmospheric circulation associated with dry conditions is mostly focused on the eastern Mediterranean and Iran (Oikonomo et al., 2010; Raziei et al., 2012; Ghassabi et al., 2021), leaving a large part of the Middle East understudied.

To summarize, while previous studies have investigated the influence of the MJO and midlatitude Rossby wave dynamics on Middle Eastern precipitation variability separately of one another, it remains unclear how the combination of these tropical and extratropical forcing mechanisms modulate the precipitation. Specifically, it is unclear whether the MJO influences Middle Eastern precipitation via a response in midlatitude Rossby wave forcing or whether these two forcing mechanisms operate

https://doi.org/10.5194/egusphere-2026-5324
Preprint. Discussion started: 9 September 2026

largely independent of one another. This study investigates the separate and joint influence of the MJO and Rossby wave dynamics on daily to multi-day precipitation variability in the Middle East during the wet season (November to April) and explores the underlying mechanisms. First, we explore the signatures in tropical and extratropical circulation based on wet and dry events in the Middle East. Second, we quantify the influence of the MJO on Middle Eastern precipitation variability at local and spatially aggregated scales and explore the underlying mechanism via tropical and extratropical circulation pathways. Third, we determine the concurrent influence of the MJO and extratropical Rossby wave dynamics on Middle Eastern precipitation variability and associated atmospheric conditions.

The manuscript is outlined as follows. Section 2 describes the employed data, methods, and diagnostics. Section 3 explores the signatures of Middle Eastern wet and dry events in the tropical and extratropical circulation patterns. Section 4 quantifies the influence of the MJO on Middle Eastern precipitation variability at local and spatially aggregated scales, and examines the underlying mechanisms by revisiting the baroclinic response in the regional (sub)tropical circulation and by exploring the influence of the MJO on Rossby wave dynamics via the regional tropical circulation and the circumglobal extratropical circulation. Section 5 quantifies the concurrent influence of the MJO and Rossby wave dynamics on Middle Eastern precipitation variability and accompanying atmospheric conditions. The study is concluded by summarizing the results in section 6.

2. Data and methodology

2.1 Datasets and MJO events

This study uses several observation-based datasets for quantifying Middle Eastern precipitation variability and the underlying atmospheric processes for the period of 1979-2020. We use daily precipitation from the Multi-Source Weighted Ensemble Precipitation (MSWEP) version V280 dataset, which is based on a combination of precipitation from reanalysis, satellite-based estimates, and station observations (Beck et al., 2019). Furthermore, we use ERA5 reanalysis data from the European Centre for Medium-Range Weather Forecasts (ECMWF) for studying the atmospheric processes linked to precipitation variability (Hersbach et al., 2020). To determine the influence of the MJO, we use daily values of the real-time multivariate MJO (RMM) index (Wheeler and Hendon, 2004), retrieved from the Australian Bureau of Meteorology. The RMM index describes the location and strength of anomalous tropical convection and circulation by eight phases and its amplitude. MJO events of each phase are defined by periods with an RMM amplitude greater than or equal to unity that persist for at least three consecutive days in that phase.

2.2 Wet and dry events

To identify wet and dry events in the Middle East, we define a target region based on objective hydroclimatic conditions. This target region is also used for quantifying the influence of the MJO and Rossby wave dynamics on spatially aggregated

https://doi.org/10.5194/egusphere-2026-5324
Preprint. Discussion started: 9 September 2026

variability in precipitation across the region. The target region is defined as the area of 10-70°E and 15-45°N and includes only grid points that (1) receive more than 80% of their annual precipitation in the MSWEP data during the wet season (November to April), (2) have an arid to hyper-arid climate, defined by aridity index values, computed as the ratio of precipitation over evapotranspiration in monthly CRU data (Haris et al., 2020), falling below 0.2, and (3) represent land area (Fig. 1a). These criteria focus the target region on the area where precipitation formation is primarily governed by midlatitude forcing during the cool season – opposed to precipitation forming under the influence of the Inter-tropical convergence zone and monsoons during the warm season – and where precipitation is relatively scarce and thus has important socio-environmental relevance. This definition follows De Vries et al. (2026) but excludes the transitions months October and May. During these months, the circulation patterns of wet and dry events differ somewhat compared to those of the core wet season months from November to April (not shown), suggesting a relatively weak and spatially varying influence of the MJO and midlatitude forcing on Middle Eastern precipitation during these transition months.

Wet and dry events are defined by anomalous precipitation amounts at daily timescales relative to climatology. Specifically, wet events are defined by at least two consecutive days with spatially aggregated precipitation exceeding 100% from climatology (i.e., a doubling). Likewise, dry events are defined by at least two consecutive days with spatially aggregated precipitation falling below 10% of climatology (i.e., a reduction by more than 90%). The climatological baseline is defined by a 21-day running mean of spatially aggregated precipitation to remove the strong seasonal cycle in precipitation over the region, allowing for the evaluation of variability in precipitation at daily timescales relative to climatological conditions for that time of the year (Fig. 1b). While it can be argued that a typical day in the Middle East remains dry, it should be kept in mind that wet and dry events are not defined locally but based on a large area. Furthermore, while we recognize that the persistence of dry days (i.e., dry spells) matters, we intentionally define dry events using the same duration criterion as for wet events to ensure symmetry of the analysis and to facilitate the comparison between wet and dry events.

2.3 Diagnostics for identifying Rossby wave packets and Rossby wave breaking

The influence of extratropical forcing on Middle Eastern precipitation is assessed by exploring the evolution of Rossby wave packets (RWP) and Rossby wave breaking (RWB). Local RWP amplitudes in space and time are diagnosed based on meridional wind fields filtered to wavelengths between 2,000 and 10,000 km, following Fragkoulidis et al. (2020). This diagnostic considers the envelope of absolute values of meridional wind and does not contain information on the phase of the transient Rossby wave packets (troughs and ridges). Existing research pointed to RWPs as upstream precursors of precipitation events in many parts of the world (Ali et al., 2021), including the southern Alps (Martius et al., 2008; Grazzini et al., 2021), Australia (Tozer et al., 2018), and South America (Matis et al., 2024).

Additionally, we consider RWB as this atmospheric process is a key driver of heavy precipitation events across the broader Middle East during the wet season (De Vries et al., 2018). We adopt the algorithm from De Vries et al. (2024), which is based

https://doi.org/10.5194/egusphere-2026-5324
Preprint. Discussion started: 9 September 2026

on the method originally introduced by Wernli and Sprenger (2007). This algorithm identifies elongated and isolated structures in potential vorticity (PV) contours at the dynamic tropopause, referred to as PV streamers and cut-off lows, respectively, serving as indicators of RWB. We compute PV fields from ERA5 data on model levels and interpolate these onto isentropic surfaces between 275-360K with 5K intervals. For identifying PV streamers and cutoff lows, we use contour lines of 2 PV units (PVU; 1 PVU = $1*10^{-6}$ kg K^{-1} m^2 s^{-1}) demarcating the boundary between tropospheric and stratospheric air masses. PV streamers are based on geometric criteria with a minimum spherical length of 1,000 km, a maximum width of 1,500 km, and a ratio of length over width larger than 1 (De Vries et al., 2018, De Vries, 2021). PV cutoff lows are tested on specific and relative humidity to remove structures resulting from diabatic processes and to only retain those of stratospheric origin (Portmann et al., 2021). For more details on this diagnostic, we refer to De Vries et al. (2024). Hereafter, PV streamers and cut-off lows with stratospheric air masses (PV > 2 PVU) are referred to as stratospheric PV structures.

2.4 Anomalous Rossby wave breaking events

In a similar way to that for wet and dry events, we also define events with anomalous Rossby wave breaking occurrence. For this purpose, we compute daily timeseries of spatially averaged vertically aggregated stratospheric PV structure occurrences across isentropic surfaces between 300-350K in the 25-45°E and 20-40°N domain. As for wet and dry events, we account for seasonality by computing anomalies in daily values from climatology by using a 21-day running mean. Events with anomalously high or low Rossby wave breaking occurrence are defined by consecutive days on which the spatially averaged running mean anomalies exceed +1 or fall below –1 standard deviation from climatology, respectively. Different from wet and dry events, we include Rossby wave breaking events of any duration, including events that last one day only.

2.5 Compositing and significance testing

We construct composites of anomalies in precipitation and the atmospheric circulation to examine the influence of the MJO and extratropical Rossby wave dynamics on rainfall variability in the Middle East. To this end, we compute for each day or 6-h time step the anomalies with respect to a 21-day running mean to remove the seasonal cycle, consistent with our approach for defining wet and dry events and anomalous RWB events. Composites are constructed based on wet and dry events, MJO events, and anomalous RWB events. To test these composites for statistical significance, we apply a Monte Carlo test by drawing random days from the period under consideration (November to April, 1979 to 2020) corresponding to the sample number on which the composites are based. This procedure is repeated 1,000 times to construct a null hypothesis assuming no relation between the event under consideration and precipitation or the atmospheric circulation anomalies. Statistical significance is then evaluated by comparing the observed value against the random distribution and applying a two-sided test at the $p < 0.05$ level, i.e., deeming observed values in the lower or upper 2.5 percentiles significant, unless mentioned otherwise. For analyses based on 4-day or 5-day episodes, we adopt the same procedure whereby randomly drawn samples also consist of equivalent multi-day chunks to ensure an adequate statistical evaluation.

https://doi.org/10.5194/egusphere-2026-5324
Preprint. Discussion started: 9 September 2026

3. A wet and dry event perspective on tropical and extratropical forcing

Atmospheric circulation composites based on wet events in the Middle East reveal key signals in both the extratropical and tropical circulation (Fig. 2). In midlatitudes, a Rossby wave train emerges over a region spanning from the eastern North Atlantic to Southwest Asia (Fig. 2a). At the onset of wet events (i.e., the first day of a wet event), a vigorous dipole in the upper-tropospheric meridional winds manifests over the Middle East with strong northerly and southerly winds over the eastern Mediterranean and northern Arabian Peninsula, respectively. This configuration of upper-tropospheric winds reflects the presence of a strong upper-level trough, commonly observed during heavy precipitation events in the region (Evans and Smith, 2006; Kumar et al., 2015; De Vries et al., 2018). Consistent with this notion, Rossby wave breaking frequencies are increased at this location by over 100% from climatology (purple hatching in Fig. 2a). Time lagged composites of Rossby wave packet amplitude anomalies reveal that the Rossby wave train originates from the North American continent approximately five days prior to the onset of wet events (Fig. 2b). The wave train propagates eastward over the North Atlantic, Europe, North Africa, the Middle East, and South Asia, and then decays over the Pacific approximately 5-8 days after the wet event onset. This wave train demonstrates noteworthy characteristics, well-known from theory (Wirth et al., 2018), moving northeastward over the North Atlantic followed by propagation in a southeastward direction prior to the precipitation event onset (not shown), reflecting a turning latitude, and then propagating eastwards, while being trapped within the subtropical jet over North Africa, the Middle East, and South Asia (Fig. 2a,b).

In the tropics, we observe a tripole pattern in anomalous outgoing longwave radiation (OLR), indicative of suppressed tropical convection over the eastern Indian Ocean and Maritime Continent and enhanced tropical convection over Equatorial Africa and the Central Pacific (Fig. 2a). Coherent eastward propagation of these anomalies during a -15 to +25 day lag window with respect to the wet event onset suggests a strong link to the MJO (Fig. 2c). Consistent with these tropical OLR anomalies, we observe westward and eastward atmospheric moisture transport anomalies over the Indian Ocean and Pacific Ocean, respectively (Fig. 2a). Over the western Indian Ocean, the anomalous westerly moisture transport turns in a northward direction into the Middle East, providing moisture supply for precipitation formation in a region that coincides with the eastern flank of equatorward breaking Rossby waves (Fig. 2a). Thus, the composites demonstrate that Middle Eastern wet events are linked to eastward propagating Rossby waves breaking into low latitudes and intraseasonal variability in tropical convection associated with the MJO.

For dry events, we observe similar atmospheric circulation patterns as for wet events but of opposite sign. (Fig. 3). In midlatitudes, a Rossby wave train emerges again in a domain spanning from the northeastern Atlantic to Southwest Asia (Fig. 3a) with some noteworthy distinct characteristics from wave trains during wet events (Fig. 2a): The dry-event wave train demonstrates a strong northeastward propagation over the North Atlantic and Europe followed by strong southeastward propagation towards lower latitudes farther to the east. Importantly, this wave train imposes a ridge over the Middle East region

https://doi.org/10.5194/egusphere-2026-5324
Preprint. Discussion started: 9 September 2026

evident from the strong southerly upper-tropospheric winds over the eastern Mediterranean and northerly winds over the Zagros Mountains and Iranian Plateau and from reduced Rossby wave breaking frequencies over the broader eastern Mediterranean (Fig. 3a). Similar to the wet events, this wave train originates from eastern North America, moves eastwards across the North Atlantic, Europe, the Middle East, and South Asia, and then decays over the Pacific in a period spanning from approximately 5 days before to 8 days after the dry-event onset (Fig. 3b). Note that the dry-event wave train is clearly visible in the 250-hPa meridional wind anomalies but features negative RWP amplitude anomalies (Fig. 3a,b), suggesting that it is not the amplitude but the phase of the Rossby wave that is critical for bringing about dry conditions over the Middle East. Another noteworthy difference compared to wet events is that the dry-event wave train exhibits eddies with stronger quasi-stationary behavior, remaining in place throughout the duration of the wave train passing by (Fig. 3b). In the tropics, OLR anomalies indicate enhanced convection over the eastern Indian Ocean and Maritime Continent and reduced convection over equatorial Africa and the Central Pacific (Fig. 3a). The eastward progression of these anomalies at intraseasonal timescales clearly points to a dominant role of the MJO but being in opposite phase compared with wet events (Fig. 3c). Anomalous atmospheric moisture transport is primarily westerly over the Indian Ocean and northeasterly over the Middle East (Fig. 3a), suggesting weakened moisture transport into the region given that the climatological mean moisture transport is from southwesterly directions.

A month-by-month comparison of composites based on wet events generally shows very similar signals in the extratropical and tropical circulation, suggesting that extratropical Rossby wave packets and MJO-like tropical convection anomalies play a central role in modulating Middle East precipitation anomalies during each month of the wet season (Figs. S1-6). Some noteworthy differences manifest in specific months. While wet events in all months are accompanied by extratropical Rossby wave trains passing over the Middle East and neighboring regions, their group- and phase-velocity, and their regions of origin and decay differ by month. For example, in January and March (Figs. S3, S5), Rossby wave packets originate from the northeast Pacific and North America about 7 days prior to the onset of wet events, travel over the Atlantic and Eurasian continent, and decay over the West Pacific approximately 5 days after the wet event onset, consistent with the findings of Feldstein and Dayan (2008) for the winter season. For November and April (Figs. S1, S6, respectively), the phase velocity of the Rossby wave packets is lower compared with the core winter months, likely linked to the varying background conditions of the zonal winds during the wet season. Furthermore, the seasonally varying relevance of other climate variability modes over the Indian and Pacific Oceans for Middle Eastern precipitation variability may also contribute to the month-to-month variation in atmospheric circulation patterns associated with wet events (De Vries et al., 2026).

https://doi.org/10.5194/egusphere-2026-5324
Preprint. Discussion started: 9 September 2026

4. The influence of the Madden-Julian Oscillation

4.1 Precipitation variability

Previous studies have investigated the influence of the MJO on precipitation variability across the Middle East and Southwest Asia focusing on tropical convection anomalies over the eastern Indian Ocean and Maritime Continent (Barlow et al., 2005; Nazemosadat and Ghaedamini, 2010) as well as single or combined phases of the MJO (Tippett et al., 2015; Pourasghar et al., 2015; Nazemosadat and Shahgholian, 2017; Hoell et al., 2018; Almazroui, 2023). This section synthesizes and extends previous work by quantifying how each phase of the MJO modulates precipitation variability in the Middle East at both local and regional scales, how this relationship evolves as a function of time lag with respect to the MJO event onset, and how this relationship varies during the warm and cold phases of El Niño-Southern Oscillation (ENSO).

Figure 4 shows the relative anomalies in precipitation composited on the onset of MJO events in all eight phases during pentads 0, 1, and 2, corresponding to lagged days from 0 to +4, +5 to +9, and +10 to +14, respectively. Precipitation increases in the Middle East are strongest for MJO phases 8 and 1 during pentads 0 and 1, exceeding 100% over parts of the region, i.e., a doubling from climatology (Fig. 4a,b,v,w). Conversely, the largest precipitation decreases occur for MJO phases 4 and 5 during pentads 0 and 1, falling below 75% from climatology over much of the region of interest (Fig. 4j,k,m,n). For all MJO phases, the precipitation anomalies manifest primarily over the southern and eastern portions of the target region in the Middle East and tend to move eastward with consecutive MJO phases and during the consecutive pentads, consistent with the eastward progression of the MJO.

Time lagged relative anomalies in spatially aggregated precipitation bear distinct signatures of the MJO up to three weeks after the onset of MJO events (Fig. 5a). Consistent with the 30-to-60-day periodicity of the MJO, the precipitation anomalies hold the same sign for approximately 15 to 30 consecutive days for each MJO phase, in agreement with previous research (Barlow et al., 2005). Mean precipitation increases are largest following MJO events in phases 8 and 1 approximately 4-5d after their onset exceeding 50% from climatology. In contrast, precipitation decreases are strongest on 7d and 2d following the onset of MJO events in phases 4 and 5, respectively, falling below 50% from the climatological mean.

We recognize that the MJO-related precipitation anomalies may bear underlying signatures from other climate variability modes given the well-documented influence of ENSO on both interannual precipitation variability across the Middle East (e.g., Cannon et al., 2017; Hoell et al., 2018; Alizadeh and Mousavizadeh, 2025; De Vries et al., 2026) and on the MJO characteristics (Hendon et al., 1999; Pohl and Matthews, 2007; Wei and Ren, 2019; Wang and Li, 2021). To explore how ENSO conditions modulate the MJO-Middle Eastern precipitation relationship, we separate MJO events from Fig. 5a into those occurring during El Niño and La Niña conditions (Fig. 5b,c). Under El Niño conditions, the MJO influence on Middle Eastern precipitation is less coherent (Fig. 5b), lacking the multi-day episodes with large and significant precipitation anomalies as observed

https://doi.org/10.5194/egusphere-2026-5324
Preprint. Discussion started: 9 September 2026

irrespective of ENSO phase (Fig. 5a). In contrast, under La Niña conditions, the MJO influence on Middle East precipitation variability manifests more strongly, with multi-day periods of large and significant precipitation reductions lasting well beyond 3 weeks after the onset of MJO events (Fig. 5c). These differences are consistent with the asymmetric influence of ENSO on Middle Eastern precipitation: El Niño conditions are associated with a moderate precipitation increase, primarily during autumn and to a lesser extent in spring, while La Niña conditions are linked to a strong precipitation decrease throughout the cool season (De Vries et al., 2026). While it is beyond the scope of the present study to explore this aspect further, the analysis shows that the MJO influence on Middle Eastern precipitation, particularly decreases, can be expected to be stronger under La Niña conditions than under El Niño conditions.

4.2 Revisiting the baroclinic response in the regional tropical circulation

Next, we revisit the well-documented regional circulation response through which the MJO modulates precipitation variability in the Middle East. Figure 6 presents composites of anomalies in outgoing longwave radiation (OLR), 200-hPa geopotential height, and 850-hPa horizontal wind during pentad 0 after the onset of MJO events in each of the eight phases. Consistent with the nature of the MJO, the OLR anomalies move eastward across the tropical Indo-Pacific Oceans with progressing MJO phases, corresponding to reduced tropical convection over the eastern Indian Ocean and Maritime Continent during phases 7, 8, and 1 (Fig. 6a,b,c) and enhanced tropical convection over this region during phases 3, 4, and 5 (Fig. 6e,f,g). These reduced and enhanced tropical convection anomalies go along with cyclonic and anticyclonic upper-tropospheric circulation patterns to the northwest of these anomalies, respectively, extending across South Asia and the Middle East, consistent with previous findings based on observations and model experiments (Barlow et al., 2005, 2007; Pourasghar et al., 2015; Hoell et al., 2018; Almazroui, 2023). In the lower troposphere, opposite circulation patterns manifest over the Indian Ocean and South Asia with anticyclonic circulation anomalies for MJO phases 7, 8, and 1 and cyclonic anomalies for MJO phases 3, 4, and 5. These opposed upper- and lower-tropospheric circulation patterns reflect the strong baroclinic response in the regional tropical circulation to MJO convective activity.

To further explore how the MJO shapes the thermodynamic and dynamic atmospheric conditions over the Middle East, we construct composites, in a similar fashion as Pourasghar et al. (2015), Cannon et al. (2017), and Hoell et al. (2018), but for total column water, vertically integrated horizontal water vapor transport, 500-hPa geopotential height, and 500-hPa vertical motion, and for all individual MJO phases (Fig. 7). MJO phases 7-2 demonstrate anomalous southwesterly atmospheric moisture transport, elevated atmospheric moisture content, and large-scale ascent across much of the Middle East, favoring wet conditions (Fig. 7a-d). Conversely, MJO phases 3-6 feature anomalous northeasterly atmospheric moisture transport, reduced moisture content, and large-scale subsidence over the region, supporting dry conditions (Fig. 7e-h). These atmospheric circulation anomalies are consistent with the Matsuno-Gill-type response to tropical convection anomalies (Matsuno, 1966; Gill, 1980) as suggested by several previous studies (Barlow et al., 2005, 2007; Hoell et al., 2012). Furthermore, Barlow et al. (2005, 2007) argued that the circulation response over the Middle East to tropical convection anomalies in the eastern Indian

https://doi.org/10.5194/egusphere-2026-5324
Preprint. Discussion started: 9 September 2026

Ocean during the cool season is analogous to the monsoon-desert mechanisms of Rodwell and Hoskins (1996, 2001), which explains how the South Asia monsoon imposes large-scale subsidence and dry conditions over the eastern Mediterranean and Middle East throughout summer (Tyrlis et al., 2013). While the MJO-related tropical convection anomalies during the cool season occur much farther south than the Asian summer monsoon convection, the southerly shift of westerlies during the cool season enables an equivalent response in the regional circulation to MJO-related tropical convection (Barlow et al. 2005, 2007).

While the above-described baroclinic response in the regional circulation to MJO convective activity has been pointed out by several previous studies, a potential influence of the MJO on Middle Eastern precipitation operating via extratropical weather systems has only been marginally explored. Barlow et al. (2005) proposed future research to assess whether the MJO influences the intensity and number of midlatitude storms passing through Southwest Asia. Accordingly, Cannon et al. (2017) examined the influence of the MJO on tracked westerly disturbances related to winter precipitation in the western Himalaya. In the next two sections, we will examine whether the MJO influences extratropical Rossby wave dynamics in the form of anomalous RWP amplitude and RWB occurrence over the Middle East. First, we will evaluate a possible immediate response resulting from an altered background flow due to the baroclinic perturbation in the regional tropical circulation (Section 4.3). Second, we will explore a possible lagged response via an extratropical circulation pathway (Section 4.4).

4.3 Immediate influence on Rossby wave dynamics via the regional tropical circulation?

To evaluate an immediate influence of the MJO on Rossby waves propagating into and breaking over the Middle East, we construct composites of anomalous RWP amplitude and RWB occurrence during wet and dry events and compare the observed signals against those in composites of MJO events in all eight phases (Figs. 8 and 9). Specifically, we consider the anomalous RWP amplitude at 250 hPa (Fig. 8a) and in a zonal mean (20-60E) vertical cross section (Fig. 8b) during pentad 0 of wet events. Consistent with Fig. 2a, RWP amplitudes are increased compared with climatology on the poleward side of the jet (Fig. 8a) and underneath the jet core extending towards the surface (Fig. 8b). Conversely, for dry events, RWP amplitudes are reduced on the poleward side of the jet and underneath the jet core (Fig. 8k,l). Comparing these patterns of wet and dry events to those of MJO events shows little resemblance. For instance, MJO phases 7, 8, and 1 demonstrate increased RWP amplitudes far equatorward of the jet (Fig. 8c-h), contrasting with increased RWP amplitudes poleward and beneath the jet core as observed during wet events Fig. 8a,b). Likewise, MJO phases 3-5 feature reduced RWP amplitudes far equatorward of the jet (Fig. 8m-r), different from the significant decrease in RWP amplitude poleward and underneath the jet core as observed during dry events (Fig. 8k,l). MJO phase 5 even shows a significant positive anomaly in RWP amplitude in the region where negative anomalies would be expected based on dry conditions (Fig. 8q,r). Thus, while the MJO affects the upper-tropospheric circulation over the broader Middle East, this influence does not modulate RWP amplitudes over the region in a manner that is consistent with wet and dry events. Therefore, we find no evidence of the MJO shaping Middle Eastern precipitation variability through an immediate influence on Rossby waves propagating into the Middle East region.

https://doi.org/10.5194/egusphere-2026-5324
Preprint. Discussion started: 9 September 2026

Given that RWPs contain both phases of a wave, that is, troughs and ridges, which typically have an opposing influence on precipitation formation, we repeat the same analysis, but for RWB occurrences, representing the trough phase of Rossby waves only (Fig. 9). Previous case studies and climatological analyses have demonstrated a key role of RWB for the formation of precipitation and extreme precipitation events in different parts of the Middle East (Evans and Smith, 2006; Kumar et al., 2015; Vries et al., 2016; 2018; Tuel et al., 2022; Sandler et al., 2024; Francis et al., 2025). Figure 9a,b shows that wet events are associated with an equatorward displacement of the subtropical jet, evident from positive and negative zonal wind anomalies at the equatorward and poleward flank of the jet stream, respectively, consistent with De Vries et al. (2026). These zonal wind anomalies extend into the lower troposphere and go along with increased RWB occurrences on the poleward side of the jet and beneath the jet core (Fig. 9a,b). Conversely, for dry events, the subtropical jet is displaced poleward going along with decreased RWB occurrences poleward and beneath the jet core (Fig. 9k,l). Similar to the composites of RWP amplitude anomalies, we find for MJO phases 7, 8, and 1 strongly increased zonal winds on the equatorward side of the jet and somewhat weakened zonal winds within the jet core (Fig. 9c-h). However, these zonal wind anomalies do not resemble the observed patterns of wet events. Notably, RWB occurrences at the poleward side and beneath the jet are significantly decreased for MJO phases 7 and 8 and significantly increased for MJO phase 2. For MJO phases 3-5, we observe strongly weakened zonal winds on the equatorward side of the jet and strengthened zonal winds in the left exit region of the jet (Fig. 9m-r) substantially differing from the patterns of dry events (Fig. 9k,l). Similarly, significant reductions in RWB occurrence are virtually absent in regions where such signals would be expected based on the dry event composites.

The overall disparity between patterns of wet and dry events with those of MJO events suggests that the MJO influence on Middle Eastern precipitation does not operate through an immediate response in Rossby waves propagating into and breaking over the Middle East. Nevertheless, the contrast between negative anomalies in RWB occurrence for MJO phases 7 and 8 and positive anomalies in RWB occurrence for MJO phase 2 is noteworthy given that both MJO phases are associated with a precipitation increase. Returning to Fig. 6 shows that, as the region of reduced tropical convection moves into the West Pacific, a region of enhanced tropical convection establishes over the Indian Ocean during MJO phase 2 (Fig. 6d). Consistent with the Matsuno-Gill mechanism, an upper-tropospheric anticyclonic circulation anomaly forms over the southern Arabian Peninsula, suggesting an apparent contradiction with the precipitation increase over the Middle East during this phase. However, Fig. 7b shows that MJO phase 2 is also accompanied by a mid-tropospheric cyclonic circulation anomaly over the Middle East with large-scale ascent on its eastern flank, consistent with the observed increases in RWB occurrence (Fig. 9i,j). These notions suggest a transition from a tropically-excited baroclinic circulation anomaly to an equivalent barotropic circulation anomaly over the Middle East as the MJO progresses from phase 7 to phase 2. In line with this suggestion, Cannon et al. (2017) showed that the MJO influence on winter precipitation variability in the western Himalaya transits from thermodynamic influence (moisture) during MJO phases 7 and 8 to dynamic forcing (westerly depression activity) during MJO phases 3 and 4.

4.4 Lagged influence on Rossby wave dynamics via an extratropical pathway?

Previous studies pointed to a strong midlatitude Rossby wave response to MJO phases 2, 3, 6 and 7 propagating from the North Pacific across North America into the North Atlantic basin (Tseng et al., 2019; Zhou et al., 2021; Quinting et al., 2024). MJO phases 3 and 7 are of particular interest to Middle Eastern precipitation variability as these phases mark the start of dry and wet conditions, respectively. To explore a possible extratropical pathway through which the MJO influences Middle Eastern precipitation, we construct composites of 200-hPa and 850-hPa geopotential height anomalies during pentads 0, 1, 2 and 3 for MJO phases 7 and 3 (Figs. 10 and 11).

MJO phase 7 convective activity over the West Pacific initiates a Rossby wave response arching northeastward over the North Pacific and towards North America (Fig. 10a). This wave train features an anticyclonic circulation anomaly over the subtropical West Pacific and a cyclonic anomaly over the central North Pacific midlatitudes during pentad 0 (Fig. 10a). During pentad 1, a strong anticyclonic circulation anomaly builds over the high latitudes of North America (Fig. 10b), followed by a cyclonic anomaly over central and northern Europe during pentads 2 and 3 (Fig. 10c,d). Farther downstream, during pentad 3, an anticyclonic circulation anomaly emerges over central Asia and a cyclonic anomaly over the Middle East (Fig. 10d). Note that the cyclonic circulation anomaly over the Middle East differs from the non-significant circulation patterns observed during pentad 0 of MJO phase 2 (not shown) and is therefore unlikely to result from the immediate response in the regional tropical circulation of the eastward progressing MJO. Evidence of the extratropical pathway is further supported by same-signed anomalies in the upper- and lower-troposphere, indicative of an equivalent barotropic Rossby wave response in an eastward direction, reaching from the North Pacific to the Eurasian continent (Fig. 10a-d). Importantly, whereas the 200-hPa and 850-hPa geopotential height anomalies over the Middle East feature negative and positive anomalies during pentad 0, respectively, these anomalies both have a negative sign during pentad 3, suggesting a change from a baroclinic circulation anomaly to an equivalent barotropic circulation anomaly over the Middle East.

Switching our attention to MJO phase 3, we find a similar Rossby wave response across the Northern Hemisphere but of opposite sign (Fig. 11). This wave train features alternating cyclonic and anticyclonic circulation anomalies over the North Pacific and the west coast of North America during pentad 0 (Fig. 11a). The cyclonic circulation anomaly over the North American west coast strengthens, followed by a Rossby wave train propagating across North America, the North Atlantic, and Europe during pentads 1 and 2 (Fig. 11b,c). Pentad 3 shows a cyclonic circulation anomaly over central Asia and an anticyclonic anomaly over the Middle East (Fig. 11d). Different from MJO phase 7, the extratropical Rossby wave train manifests much clearer over the North Atlantic and Europe for MJO phase 3. However, similar to MJO phase 7, we note a barotropic circulation anomaly over the Middle East during pentad 3 with positive 200-hPa and 850-hPa geopotential height anomalies (Fig. 11d). Note that the anticyclonic circulation anomaly over the Middle East is well separated from the

https://doi.org/10.5194/egusphere-2026-5324
Preprint. Discussion started: 9 September 2026

anticyclonic circulation anomaly over East Asia. The former exhibits characteristics of an equivalent barotropic response and the latter, located to the northwest of enhanced tropical convection over the West Pacific, of a Matsuno-Gill-type response.

Next, we focus on the regional circulation response over the Middle East to the MJO using spatially averaged anomalies in 200-hPa and 850-hPa geopotential height and stratospheric PV structure occurrences expressed as a function of MJO phase and time lag (Fig. 12b-d). While the 200-hPa and 850-hPa geopotential height anomalies show a similar evolution in time, we also note a clear shift in the upper- and lower-tropospheric anomalies with respect to MJO phase (Fig. 12b,c). Based on the difference and similarity in sign of the upper- and lower-tropospheric anomalies, we designate the circulation response as baroclinic and barotropic, respectively, expressed by red and blue rectangles overlaid in Fig. 12a, on top of the spatially aggregated precipitation anomalies as in Fig. 5a. This depiction confirms the earlier notions that the precipitation increase for MJO phase 7 concurs with a transition from a baroclinic circulation response during pentad 0 to a barotropic circulation response during pentads 2 and 3. Consistent with this pattern, RWB occurrences over the Middle East are significantly increased during lag days +15 to +19 (Fig. 12d). Similarly, dry conditions for MJO phase 3 are associated with baroclinic circulation anomalies during pentad 0 and with barotropic circulation anomalies during pentads 2 and 3 (Fig. 12a). The lagged barotropic response promoting dry conditions is more pronounced than the lagged response to MJO phase 7, extending into pentads 3 and 4 for MJO phases 1 and 2. Generally, the transition of an immediate baroclinic to a lagged barotropic circulation response is visible across MJO phases given the dominance of red rectangles during pentad 0 and prior to the onset of MJO events and the increasing dominance of blue rectangles during pentads 2, 3 and 4. Altogether, our analysis suggests that the MJO influence on Middle Eastern precipitation variability is primarily exerted through an immediate baroclinic response in the regional tropical circulation, consistent with the Matsuno-Gill model, and to a lesser extent, through a lagged response via the extratropics in the form of an equivalent barotropic Rossby wave response.

5. Concurrent influence of the MJO and Rossby wave dynamics on Middle East precipitation variability

So far, we have found that the MJO modulates Middle Eastern precipitation variability predominantly through its immediate influence via the regional tropical circulation and to a much smaller degree through a lagged response via the extratropical circulation, suggesting that tropical and extratropical forcing mechanisms operate largely independent of one another. This raises the question of how concurrent MJO events and Rossby wave dynamics govern the precipitation variability in the Middle East. To address this question, we construct composites of relative anomalies in multi-day precipitation based on events with anomalously strong and weak RWB concurring with an inactive MJO and with MJO phases 7-2 and phases 3-6 (Fig. 13), associated with precipitation increase and decreases, respectively (Figs. 4 and 5). Events with anomalously strong RWB concurring with an inactive MJO are, as expected, accompanied by a strong and significant precipitation increase across the region of interest, locally exceeding 75% (Fig. 13a). Conversely, anomalously weak RWB events concurring with an inactive MJO are characterized by a strong and significant precipitation decrease falling below -50% of the climatological mean (Fig.

https://doi.org/10.5194/egusphere-2026-5324
Preprint. Discussion started: 9 September 2026

13b). Interestingly, anomalously strong RWB events concurring with MJO events in phase 7-2 are associated with a much stronger precipitation increase than concurrence with an inactive MJO, exceeding 150% over much of the target region (Fig. 13c). Likewise, anomalously weak RWB events concurring with MJO events in phase 3-6 result in much drier conditions than concurrence with an inactive MJO, showing precipitation anomalies falling below -75% over the central Arabian Peninsula (Fig. 13f). In contrast, events with anomalously strong RWB concurring with MJO phase 3-6, and events with anomalously weak RWB concurring with MJO phase 7-2, result in weak precipitation anomalies with both positive and negative signs in different parts of the regions of interest with limited significance (Fig. 13d,e). This shows that the MJO influence can either reinforce or mute the multi-day precipitation response that can be expected from midlatitude forcing alone.

To provide process understanding of how concurrent MJO events and midlatitude Rossby wave forcing modulate Middle Eastern precipitation variability, we construct analogue composites as in Fig. 13 but with atmospheric thermodynamic and dynamic characteristics (Fig. 14). As expected, events with anomalously strong RWB, concurring with an inactive MJO, feature a mid-tropospheric cyclonic circulation anomaly centered on the Levant along with strengthened southwesterly atmospheric moisture transport, enhanced atmospheric water content, and dynamic lifting on its downstream flank, favoring wet conditions (Fig. 14a). Concurrence of anomalously strong RWB events with MJO phases 7-2 shows a similar mid-tropospheric cyclone compared with a concurring inactive MJO but with much stronger anomalous atmospheric moisture transport, larger positive anomalies in atmospheric water content, and stronger and more widespread upward motion (Fig. 14c). In contrast, anomalously strong RWB events concurring with MJO phases 3-6 are characterized by a somewhat weaker mid-tropospheric trough, weaker upward motion, and an absence of enhanced southerly moisture transport anomalies over the Arabian Sea along with near-zero to even negative anomalies in atmospheric moisture content over the Middle East (Fig. 14e). This suggests that the MJO influence can regulate the efficiency of midlatitude disturbances in generating precipitation through strengthening or suppressing moisture supply and large-scale vertical motion.

Conversely, events with anomalously weak RWB concurring with an inactive MJO demonstrate a mid-tropospheric anticyclonic circulation anomaly with anomalous northeasterly moisture transport, reduced atmospheric water content, and large-scale descent on its eastern flank, promoting dry conditions (Fig. 14b). Concurrence of anomalously weak RWB events with MJO phases 3-6 displays a similar mid-tropospheric anticyclone as with a concurring inactive MJO but with larger negative anomalies in atmospheric moisture content and more widespread subsidence (Fig. 14f). By contrast, concurrence of anomalously weak RWB events with MJO phases 7-2 show weaker northeasterly moisture transport anomalies, both positive and negative atmospheric moisture content anomalies, and limited large-scale descent over the region of interest (Fig. 14d). Altogether, the results suggest that the remote influence of the MJO can amplify or mute the precipitation response to local midlatitude Rossby wave forcing by supplying or depriving the region from southwesterly moisture transport and by imposing large-scale upward or downward motion, either reinforcing or counterbalancing the influence of breaking Rossby waves on the formation of precipitation.

https://doi.org/10.5194/egusphere-2026-5324
Preprint. Discussion started: 9 September 2026

To further quantify the influence of concurrent MJO and Rossby wave forcing on Middle Eastern precipitation, we compute the spatially averaged precipitation anomalies for days with anomalous RWB categories defined by a range in standard deviations and the eight MJO phases (Fig 15b). For reference, Fig. 15a presents the number of days falling into the respective categories of RWB anomalies and MJO phases. Consistent with the earlier analysis, concurring strong RWB with MJO phases 7-2 produce the largest precipitation increases, reaching over +100% from climatology, and concurring weak RWB with MJO phases 3-6 result in the largest precipitation decreases falling below –75% (Fig. 15b). Remarkably, MJO phases 4 and 5 are able to cancel out the precipitation increase under the largest RWB occurrence anomalies. Likewise, MJO phases 8 and 1 during anomalously weak RWB can offset dry conditions, or even result in positive precipitation anomalies. These results show that the remote influence of the MJO and local Rossby wave forcing contribute approximately equally to precipitation variability in the Middle East on daily timescales.

6. Summary

The arid climate and mountainous character of the Middle East along with the high precipitation irregularity make the region prone to both drought and flooding. Such hydrometeorological hazards - further amplified by climate change - have been suggested to spark armed conflict and displacement (Gleick, 2014; Kelley et al., 2015; Daoudry et al., 2022), and conversely, political dispute, war, and migration in the region make the population more vulnerable to these hazards (Barlow et al., 2016; Zittis et al., 2022; Coleman et al., 2026). Given that much of the annual total precipitation falls during only a few rainfall events per year, it is thus of high societal and scientific importance to better understand the atmospheric mechanisms that modulate the precipitation variability in this region. Previous studies have shown that Middle Eastern precipitation at daily timescales is strongly influenced by both extratropical forcing through Rossby waves propagating and breaking into the region (Evans and Smith, 2006; Kumar et al., 2015; Almazroui et al., 2016; De Vries et al., 2016, 2018; Tuel et al., 2022; Breeden et al., 2023; Sandler et al., 2024; Francis et al., 2025) and by intraseasonal variability in tropical convection related to the Madden-Julian Oscillation (Barlow et al., 2005, 2007; Nazemosadat and Ghaedamini, 2010; Hoell et al., 2012, 2018). However, previous work focused primarily on these extratropical and tropical forcing mechanisms in isolation, and the combined effect of these two forcing mechanisms on Middle Eastern precipitation remained largely unknown. This study quantifies the influence of the MJO and midlatitude Rossby wave dynamics on Middle Eastern precipitation variability on daily to multi-day timescales during the cool season and clarifies the underlying atmospheric mechanisms.

Our study set out by taking the perspective of wet and dry events in the Middle East, showing that both wet and dry conditions are associated with anomalous circulation patterns in the extratropical and tropical circulation, indicative of amplifying and breaking Rossby waves and MJO convective activity. An inversed approach – taking the MJO as a starting point – shows that MJO phases 7-2 are associated with precipitation increases across the Middle East and MJO phases 3-6 with precipitation decreases, in line with previous studies (Pourasghar et al., 2015, 2019; Hoell et al., 2018; Nazemodadat and Shahgholian, 2017; Almazroui, 2023). Specifically, these precipitation anomalies are largest for MJO phases 8 and 1, locally exceeding 150% above normal conditions, and MJO phases 4 and 5, falling below –75% from the climatological mean. Anomalies in spatially aggregated precipitation across the region of interest exceed 50% and fall below –50% from climatology, and persist up to three weeks after the onset of MJO events. The MJO – Middle Eastern precipitation relationship is less coherent and weaker under El Niño conditions and more persistent and stronger under La Niña conditions.

Detailed composites of atmospheric thermodynamic and dynamic conditions corroborate previous studies, showing that the MJO modulates Middle Eastern precipitation variability through a baroclinic response in the regional tropical circulation (Barlow et al., 2005, 2007; Hoell et al., 2012, 2018). Reduced tropical convection over the eastern Indian Ocean and Maritime Continent sets up an upper-tropospheric cyclonic circulation anomaly to the northwest of the convective anomaly, reaching across South Asia and the Middle East. In the lower troposphere, an anticyclonic circulation anomaly steers warm, moist air masses from the south into the region of interest. Enhanced atmospheric moisture content combined with large-scale ascent shape favorable conditions for the formation of precipitation. Conversely, enhanced tropical convection over the eastern Indian Ocean and Maritime Continent generate an upper-tropospheric anticyclonic and lower-tropospheric cyclonic circulation anomaly, linked to widespread subsidence and northeasterly advection of cold and dry air, suppressing precipitation.

While the MJO alters the atmospheric circulation over the Middle East, we find no evidence of a robust and immediate response in Rossby waves propagating and breaking into the Middle East in a manner that is consistent with the patterns observed for wet and dry events. For example, anomalies in RWP amplitudes during MJO events do not resemble the positive (negative) RWP amplitude anomalies on the poleward side and beneath the jet core as observed during wet (dry) events. Notably, RWB occurrences are decreased at the poleward flank and beneath the jet core during MJO phases 7 and 8 but increased during MJO phase 2, showing a disparity with the observed RWB occurrence increases at this location for wet events. Interestingly, the shift from negative to positive RWB occurrence anomalies during MJO phases 7 – 2, when precipitation is generally increased, aligns with a transition from a baroclinic to a barotropic atmospheric circulation anomaly over the Middle East. Composites of the midlatitude circulation for MJO events in phase 7 (phase 3) suggest an eastward propagating equivalent barotropic Rossby wave train throughout the extratropics, associated with a barotropic cyclonic (anticyclonic) circulation anomaly over the Middle East approximately two to three weeks after the onset of MJO events, extending the wet (dry) conditions initiated by the immediate baroclinic response to the respective MJO phases. Altogether, our results suggest that the MJO primarily modulates the Middle Eastern precipitation through the immediate baroclinic response in the tropical regional circulation, consistent with the Matsuno-Gill model, and to a lesser extent through a lagged response via the extratropical circulation in the form of an equivalent barotropic Rossby wave train.

https://doi.org/10.5194/egusphere-2026-5324
Preprint. Discussion started: 9 September 2026

To evaluate how the concurrent influence of the MJO and Rossby wave dynamics modulate Middle Eastern precipitation variability, we compared the coincidence of anomalously strong and weak RWB events during MJO phases 7-2 and phases 3-6 against the coincidence with an inactive MJO. Concurrent anomalously strong RWB with MJO phases 7-2 result in amplified wet conditions over the Middle East compared to concurrence with an inactive MJO. Conversely, anomalously weak RWB concurring with MJO phases 3-6 result in very dry conditions. In contrast, concurrence of anomalously strong RWB with MJO phases 3-6, and of anomalously weak RWB with MJO phases 7-2, leads to a muted precipitation response. The regional baroclinic perturbation induced by MJO convection strengthens or reduces atmospheric moisture transport into the Middle East and imposes large-scale ascent or descent, thereby regulating the efficiency of midlatitude Rossby waves in forming or suppressing precipitation. Importantly, the influence of the MJO can double or neutralize the precipitation response that would be expected from the midlatitude forcing alone. For example, whereas spatially aggregated precipitation anomalies during anomalously strong RWB are amplified during MJO phases 8 and 1, these anomalies can become negative for concurrence with MJO phases 4 and 5. Likewise, negative precipitation anomalies during anomalously weak RWB are strengthened during MJO phases 4 and 5, but can become positive for concurrence with MJO phases 8 and 1. In summary, the remote influence of the MJO modulates the daily to multi-day precipitation variability in the Middle East with a comparable magnitude as the local midlatitude Rossby wave forcing.

The reader should keep several limitations and specifics of the study in mind when interpreting the results. While the wet and dry event perspective (Sect. 3) showed similar patterns in the extratropical and tropical circulation on a monthly basis, most of analysis is based on a wet season average, and thus, the results may differ across individual months of the wet season. While the spatially aggregated anomalies in precipitation yield specific quantifications, one should bear in mind that MJO influence manifests primarily in the southern and eastern portions of the target region, and that the measured influence of midlatitude forcing may be sensitive to the specific choice of the region for defining events with anomalous RWB occurrence. While our results suggest a response in Middle Eastern precipitation via an extratropical circulation pathway, future research may substantiate these findings based on target model experiments to disentangle the lagged influence through the circumglobal midlatitude circulation from the immediate response via the regional tropical circulation.

Overall, our study contributes to improved process-understanding of tropical and extratropical forcing mechanisms of daily to multi-day precipitation variability in the Middle East during the wet season. Previous studies have emphasized that precipitation forms under the influence of tropical-extratropical interactions at synoptic scales (Kahana et al., 2002; Rubin et al., 2007; De Vries et al., 2016, 2018). Our study shows that the influence of both tropical and extratropical forcing extends beyond synoptic scales towards larger and planetary scales and from daily to sub-seasonal timescales. Our findings may help interpret and improve medium-range to sub-seasonal prediction of precipitation and assist early warnings for flood and drought hazards. Our study also provides a framework for evaluating the climate model representation and future changes of precipitation in a water-scarce and socio-politically vulnerable region.

https://doi.org/10.5194/egusphere-2026-5324
Preprint. Discussion started: 9 September 2026

Figure captions

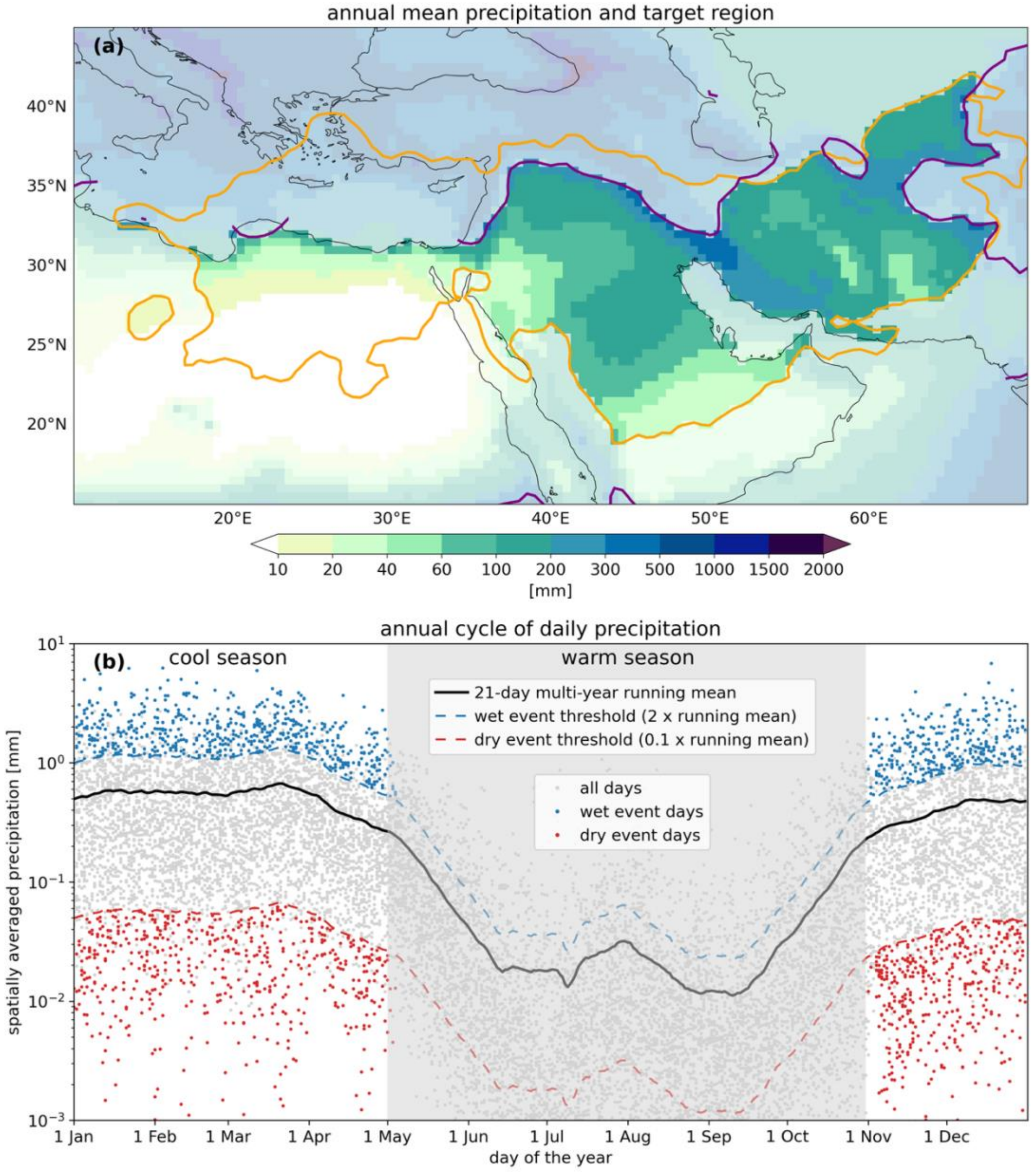

Figure 1. (a) Annual precipitation amounts (mm) from MSWEP (1979-2020) in opaque colors within the target region and in transparent colors outside the target region. Orange contours demarcate the region where more than 80% of the annual precipitation falls during the cool season (November-April), and the purple contours highlight an aridity index of 0.2, denoting the boundary between a semi-arid and arid climate. (b) Annual cycle of the daily precipitation climatology with the 21-day multi-year running mean and the thresholds to define wet and dry events in lines, and the daily precipitation amounts in dots, see the legend. Note that some days with precipitation exceeding the thresholds do not belong to wet or dry events due to the persistence criterion or due to their occurrence during the warm season (grey shading).

https://doi.org/10.5194/egusphere-2026-5324
Preprint. Discussion started: 9 September 2026

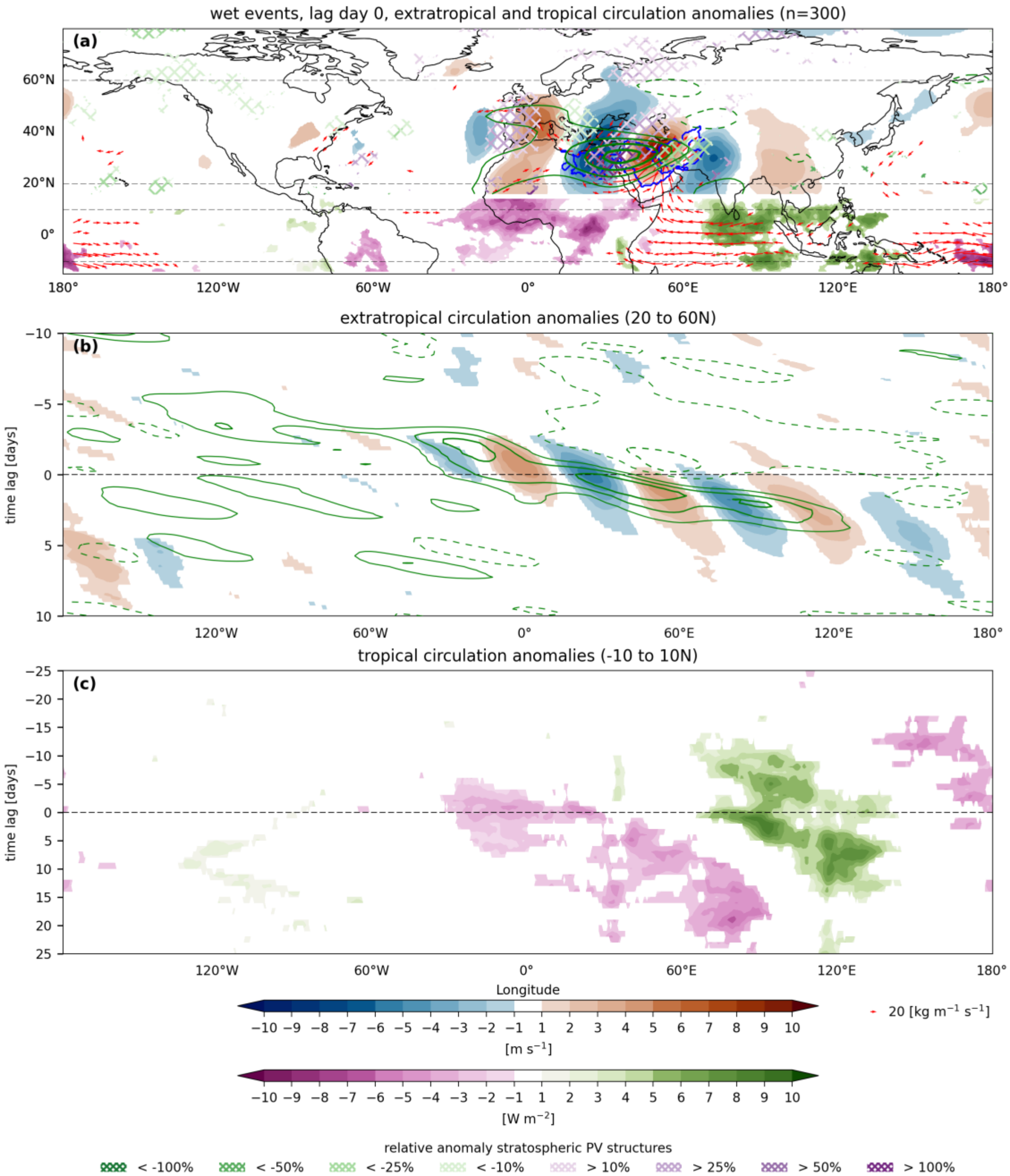

Figure 2. Composites of the atmospheric circulation based on the onset of wet events in the Middle East from November to April for the period 1979-2020. (a) Daily anomalies at lag day 0, in the extratropical domain, of 250-hPa meridional wind (m s^{-1}) in bluish-reddish colors, of RWP amplitudes (m/s) in green solid and dashed contours for positive and negative values at 1 m s^{-1} intervals, respectively, and of vertically aggregated stratospheric PV structure occurrences in green and purple hatching, see the legend; and in the tropical domain, of OLR (W m^{-2}) in purple-greenish colors (negative values indicate decreased OLR, i.e., enhanced convection, and positive values denote increased OLR, i.e., reduced convection), and in the entire domain, of vertically integrated horizontal water vapor transport (kg m^{-1} s^{-1}) in red vectors. (b) Hovmöller diagram with 6-h anomalies of 250-hPa meridional wind (m s^{-1}) in

https://doi.org/10.5194/egusphere-2026-5324
Preprint. Discussion started: 9 September 2026

colors and of RWP amplitudes (m s^{-1}) in green contours at 0.5 m s^{-1} intervals, averaged over the latitudes 20-60°N. (c) Hovmöller diagram with daily mean anomalies of OLR (W m^{-2}) averaged over latitudes 10°S-10°N. Anomalies in 250-hPa meridional wind, stratospheric PV structure occurrences, and OLR in (a-c) are only shown where statistically significant based on a Monte Carlo test with 1,000 samples and a two-sided test at the $p < 0.05$ level. Vectors in (a) are only shown where magnitudes in IVT anomalies, derived from their zonal and meridional components, exceed 20 kg m^{-1} s^{-1}.

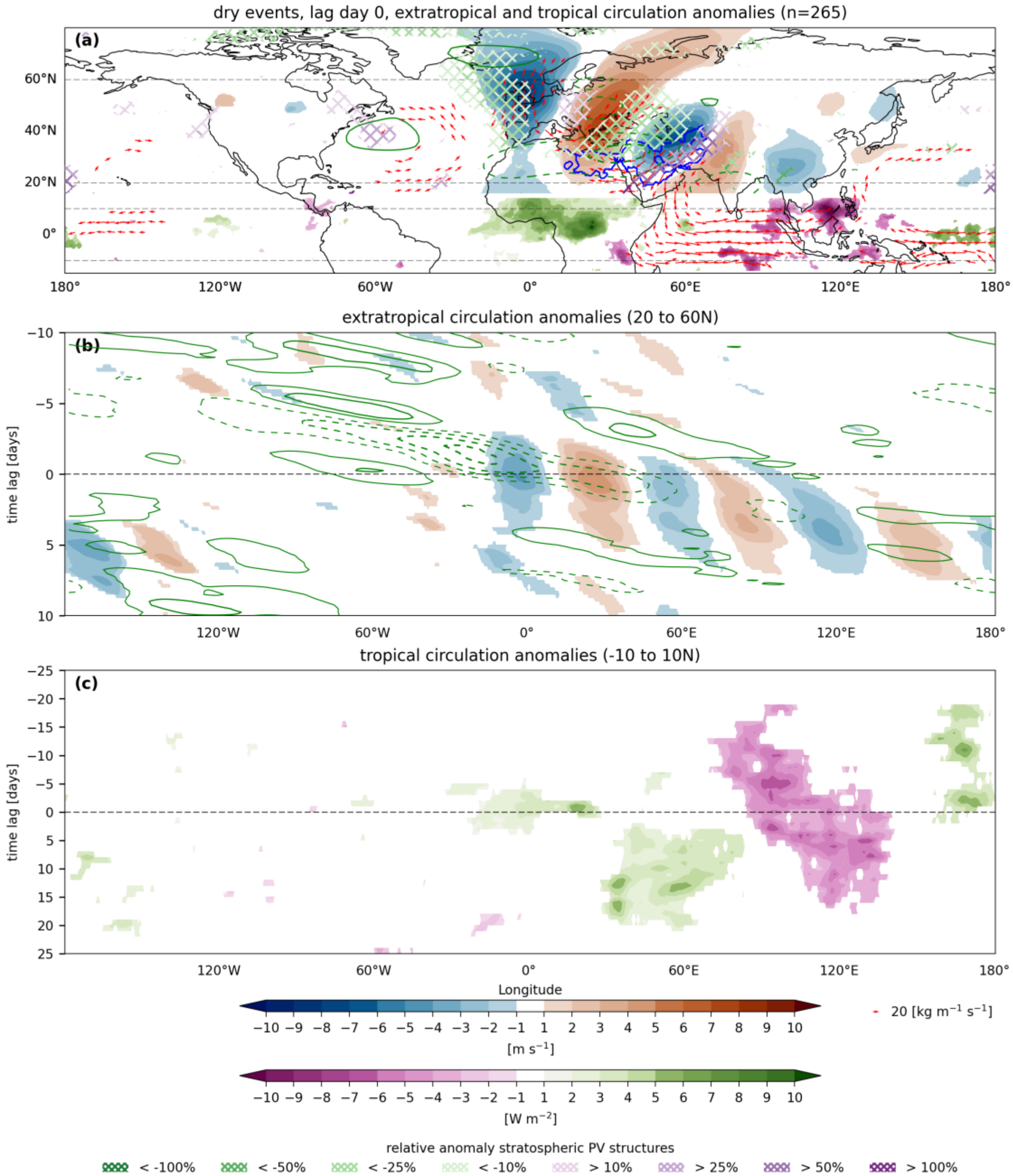

Figure 3. As Fig. 2 but with composites based on the onset of dry events.

https://doi.org/10.5194/egusphere-2026-5324
Preprint. Discussion started: 9 September 2026

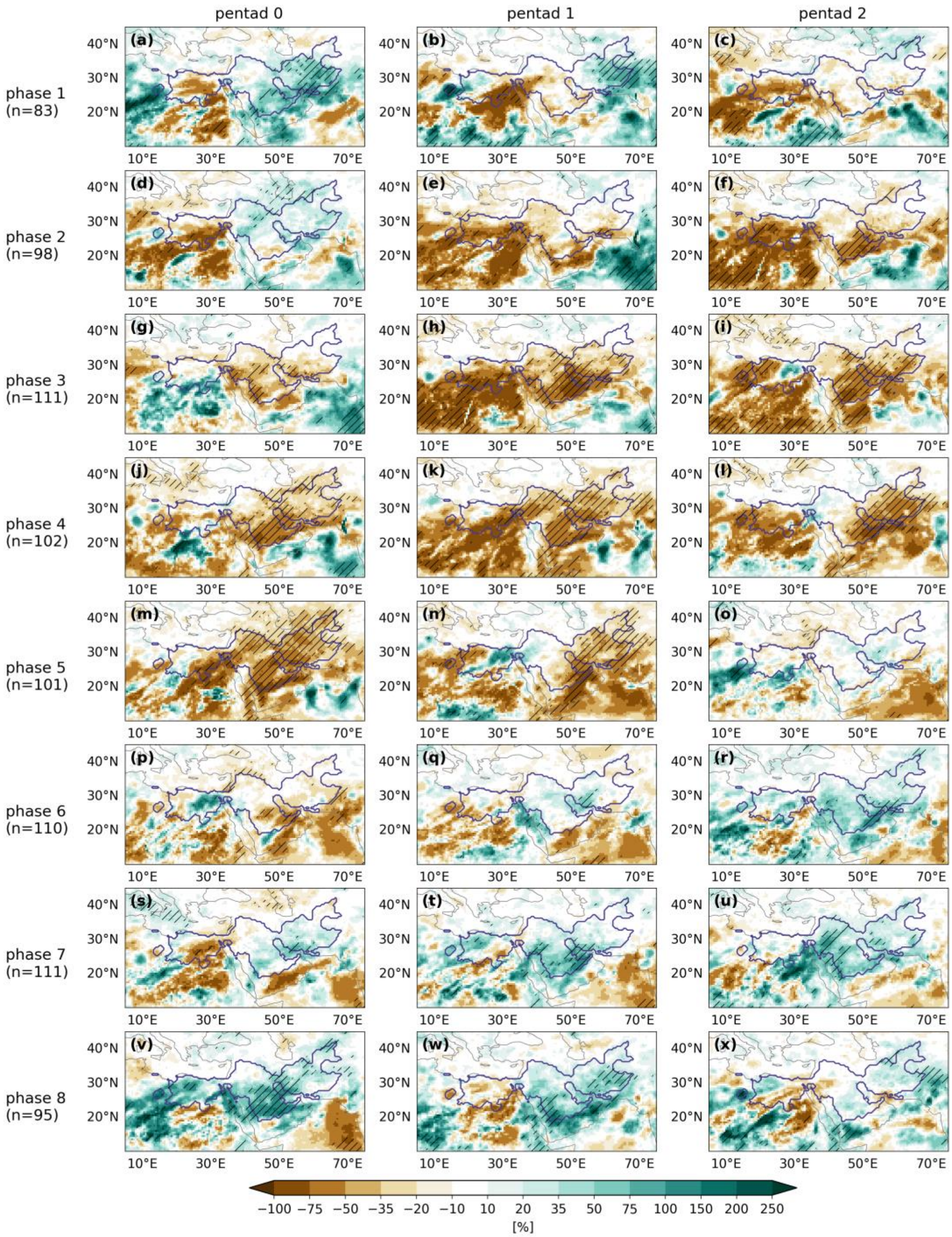

640 **Figure 4. Relative precipitation anomalies in MSWEP for MJO phases (rows) 1-8 and (left column) pentad 0, lag day 0 to +4, (middle column) pentad 1, lag day +5 to +9, and (right column) pentad 2, lag day +10 to +14. Diagonal hatching denotes statistical significance in the 5-day anomalies at the $p < 0.05$ level. For reference, the target region is indicated in purple contours, see text for details.**

https://doi.org/10.5194/egusphere-2026-5324
Preprint. Discussion started: 9 September 2026

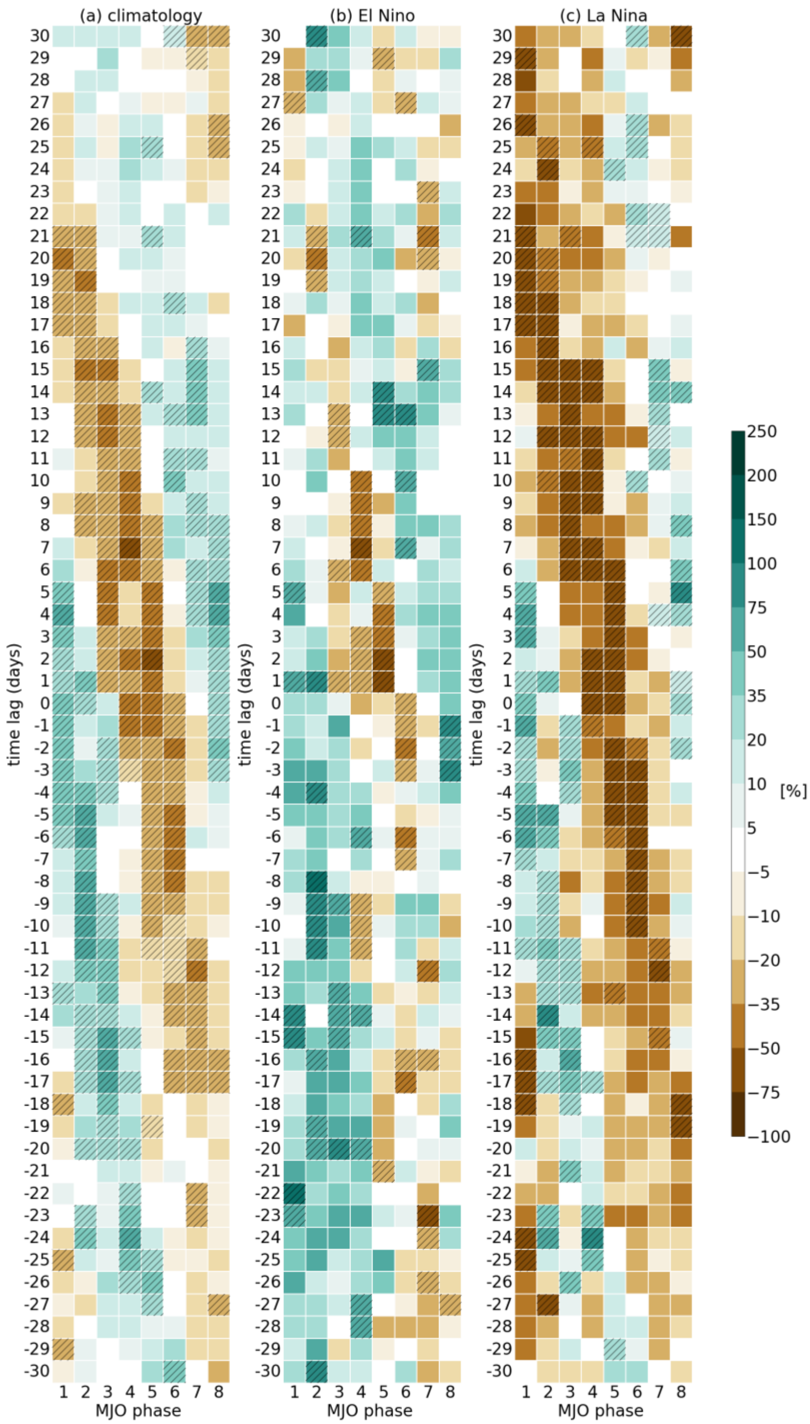

Figure 5. Relative anomalies in spatially aggregated daily precipitation over the target region for all MJO phases and time lags from -30 to +30 days with respect to the onset of MJO events for (a) all MJO events, (b) only MJO events during El Niño conditions, and (c) only MJO events during La Niña conditions. Hatching denotes statistical significance at the p < 0.1 level.

https://doi.org/10.5194/egusphere-2026-5324
Preprint. Discussion started: 9 September 2026

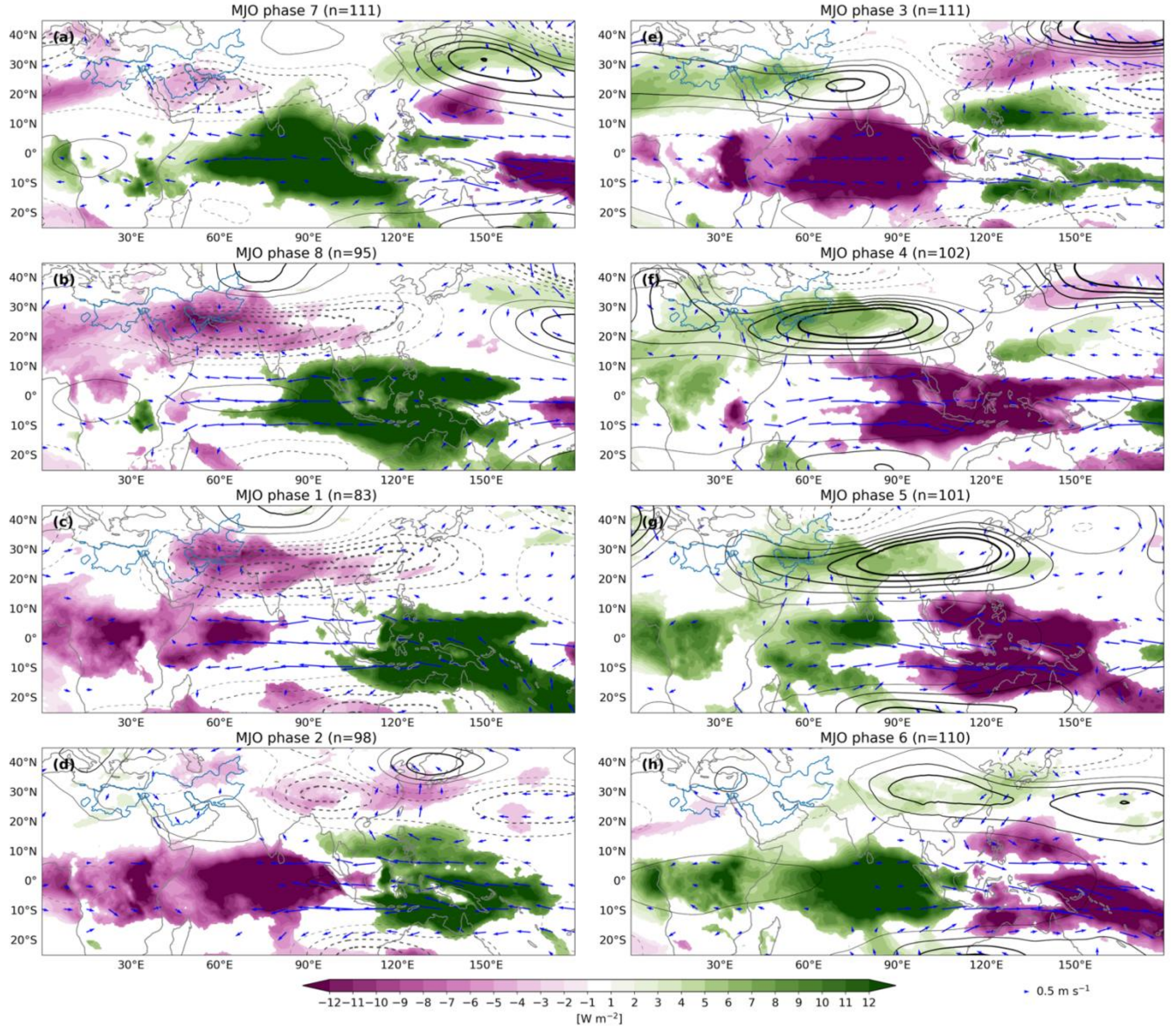

Figure 6. Composites of anomalies in OLR (W m^{-2}) in color, whereby negative values indicate enhanced convection and positive values reduced convection, in 200-hPa geopotential height (gpm) in solid and dashed black contours for positive and negative values, respectively, at intervals of 8 gpm up to 50 gpm, and in 850-hPa horizontal wind (m s^{-1}) in blue vectors for pentad 0 of MJO (a) phase 7, (b) phase 8, (c) phase 1, (d) phase 2, (e) phase 3, (f) phase 4, (g) phase 5, and (h) phase 6. OLR anomalies are only shown where significant at the $p < 0.05$ level. Wind vectors are only shown where anomalous wind speeds, derived from their zonal and meridional components, exceed 0.5 m s-^{1}. The target region is indicated in blue contours for reference.

https://doi.org/10.5194/egusphere-2026-5324
Preprint. Discussion started: 9 September 2026

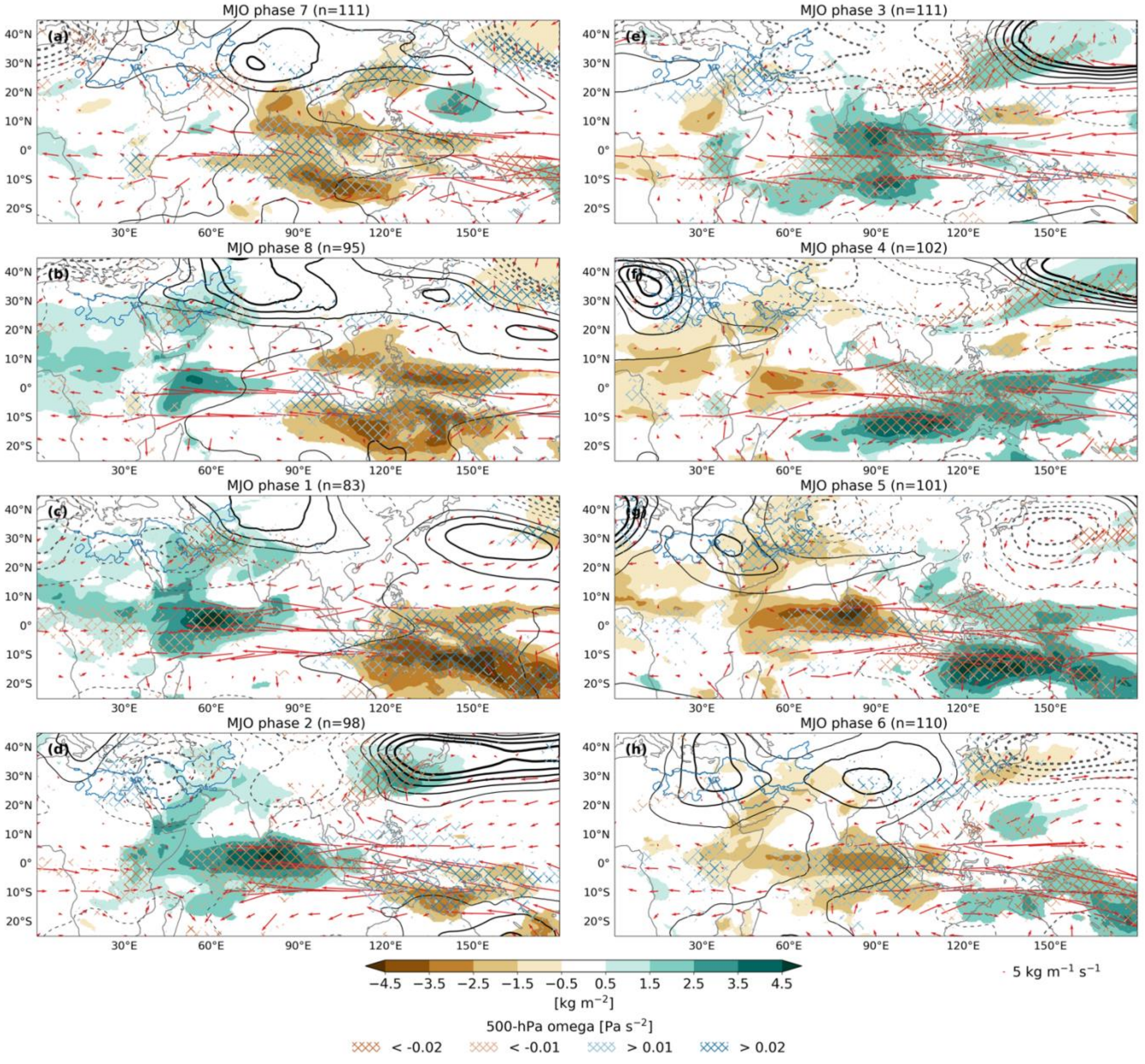

Figure 7. Composites of anomalies in total column water (kg m^{-2}) in colors, in 500-hPa geopotential height contours at 4 gpm intervals up to 20 gpm, in solid and dashed for positive and negative values, respectively, in vertically integrated horizontal water vapor transport (kg m^{-1} s^{-1}) in red vectors, and in 500-hPa omega (Pa s^{-1}) in hatching (see the legend) whereby negative values correspond to upward motion and positive values to downward motion. Panels show pentad 0 of MJO (a) phase 7, (b) phase 8, (c) phase 1, (d) phase 2, (e) phase 3, (f) phase 4, (g) phase 5, and (h) phase 6. Anomalies in total column water are only shown where significant at the $p < 0.05$ level. Red vectors are only shown where anomalous IVT, derived from their zonal and meridional components, exceed 5 kg m^{-1} s^{-1}. The target region is indicated in blue contours for reference.

https://doi.org/10.5194/egusphere-2026-5324
Preprint. Discussion started: 9 September 2026

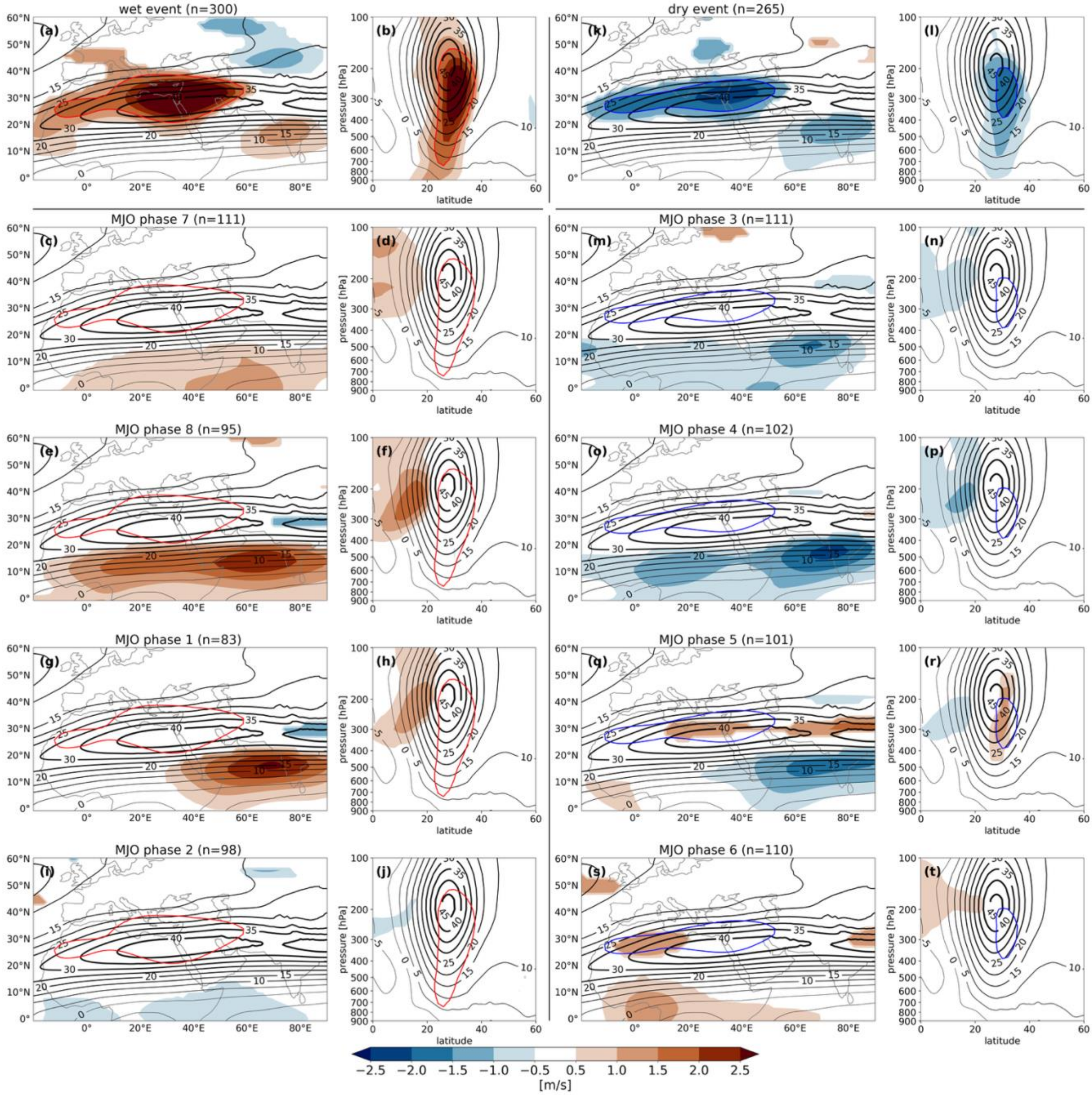

Figure 8. Composites of anomalies in RWP amplitudes for the onset day of (a,b) wet events and (k,l) dry events and pentad 0 for MJO events in (c,d) phase 7, (e,f) phase 8, (g,h) phase 1, (i,j) phase 2, (m,n) phase 3, (o,p) phase 4, (q,r) phase 5, and (s,t) phase 6. In (a,c,e,g,i,k,m,p,q,s) 250-hPa RWP amplitude anomalies in colors and the climatological mean 250-hPa zonal winds in black contours at 5 m s^{-1} intervals. In (b,d,f,h,j,l,n,p,q,t) the zonal mean (20-60°E) RWP amplitude anomalies in colors and the climatological zonal mean zonal wind in black contours. Anomalies in RWP amplitude are only shown where statistically significant at the $p < 0.05$ level.

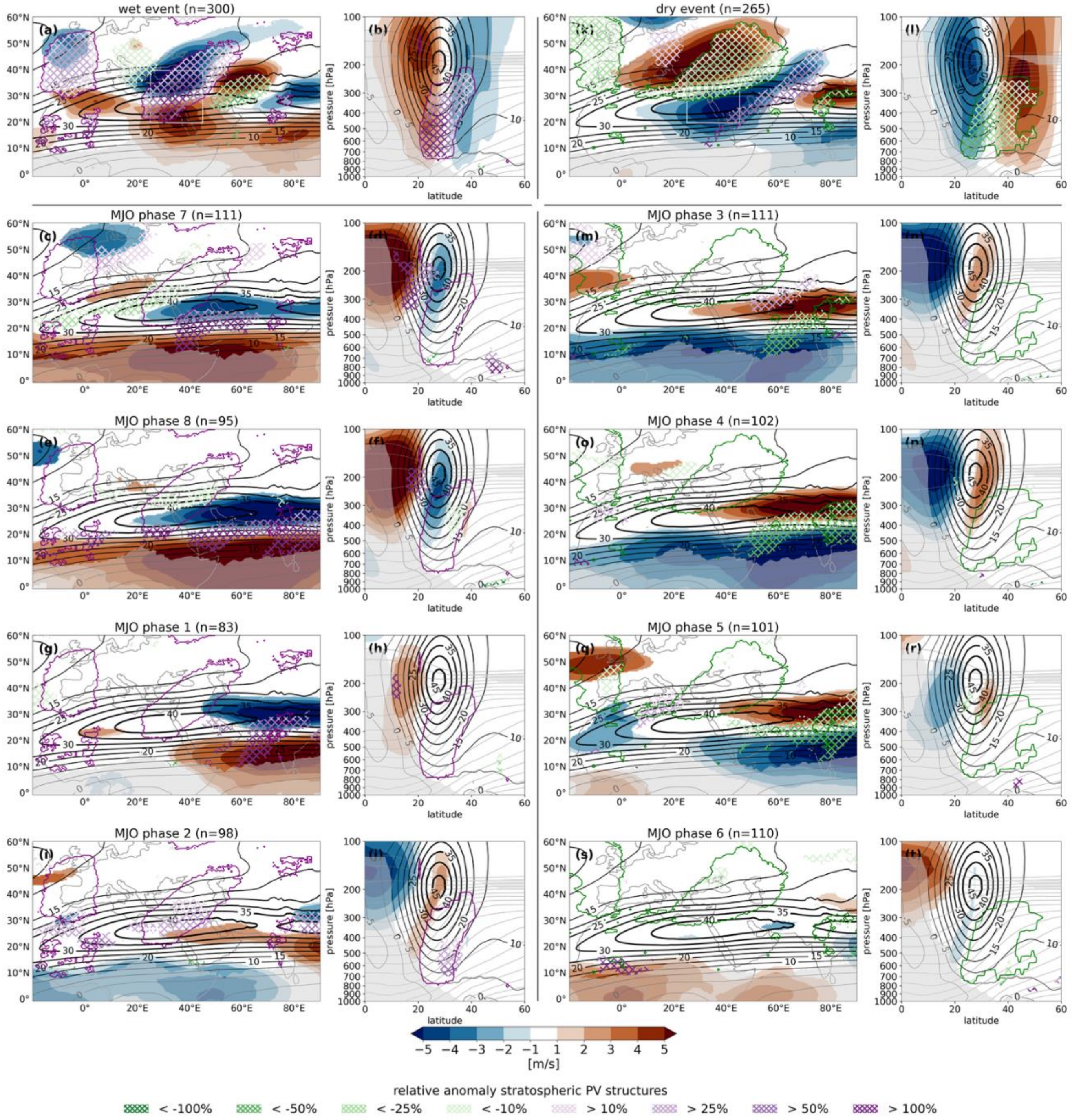

Figure 9. As Fig. 8 but with zonal wind anomalies in color and relative anomalies in stratospheric PV structure frequencies in green and purple hatching, see the legend. Stratospheric PV structure frequencies in (a,c,e,g,h,k,m,p,q,s) are based on vertically aggregated occurrences across the 300-350K isentropic surfaces, and in (b,d,f,h,j,l,n,p,q,t) on zonal mean (20-60E) occurrences across the 275-360K isentropic surfaces interpolated to pressure levels. Isentropic surfaces in zonal mean cross sections are indicated in grey contours at 5K intervals. Zonal wind and stratospheric PV structure occurrences are only shown where statistically significant at the p < 0.05 level.

https://doi.org/10.5194/egusphere-2026-5324
Preprint. Discussion started: 9 September 2026

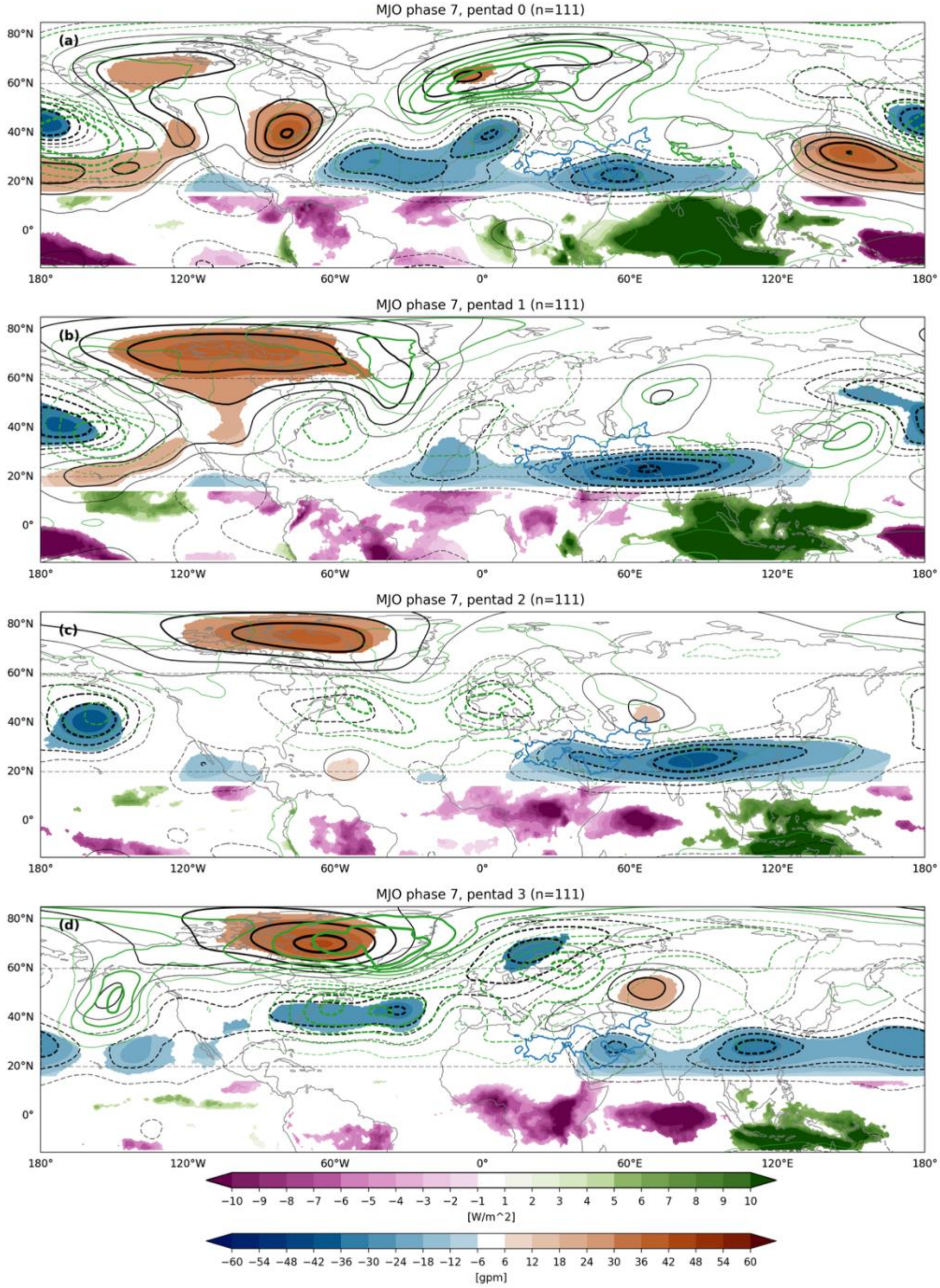

Figure 10. Composites of the circulation anomalies for MJO phase 7, (a) pentad 0, (b) pentad 1, (c) pentad 2, and (d) pentad 3, with 200-hPa geopotential height in colors, north of 16N, and in black contours at 8 gpm intervals up to 40 gpm, in solid and dashed lines for positive and negative values, respectively, throughout the domain. Anomalies of 850-hPa geopotential height are shown in green
675 **contours at 4 gpm intervals up to 20 gpm, in solid and dashed for positive and negative values, respectively, throughout the domain, and of OLR in colors, south of 14N. Anomalies in 200-hPa geopotential height and OLR in colors are only shown where statistically significant at the $p < 0.05$ level.**

https://doi.org/10.5194/egusphere-2026-5324
Preprint. Discussion started: 9 September 2026

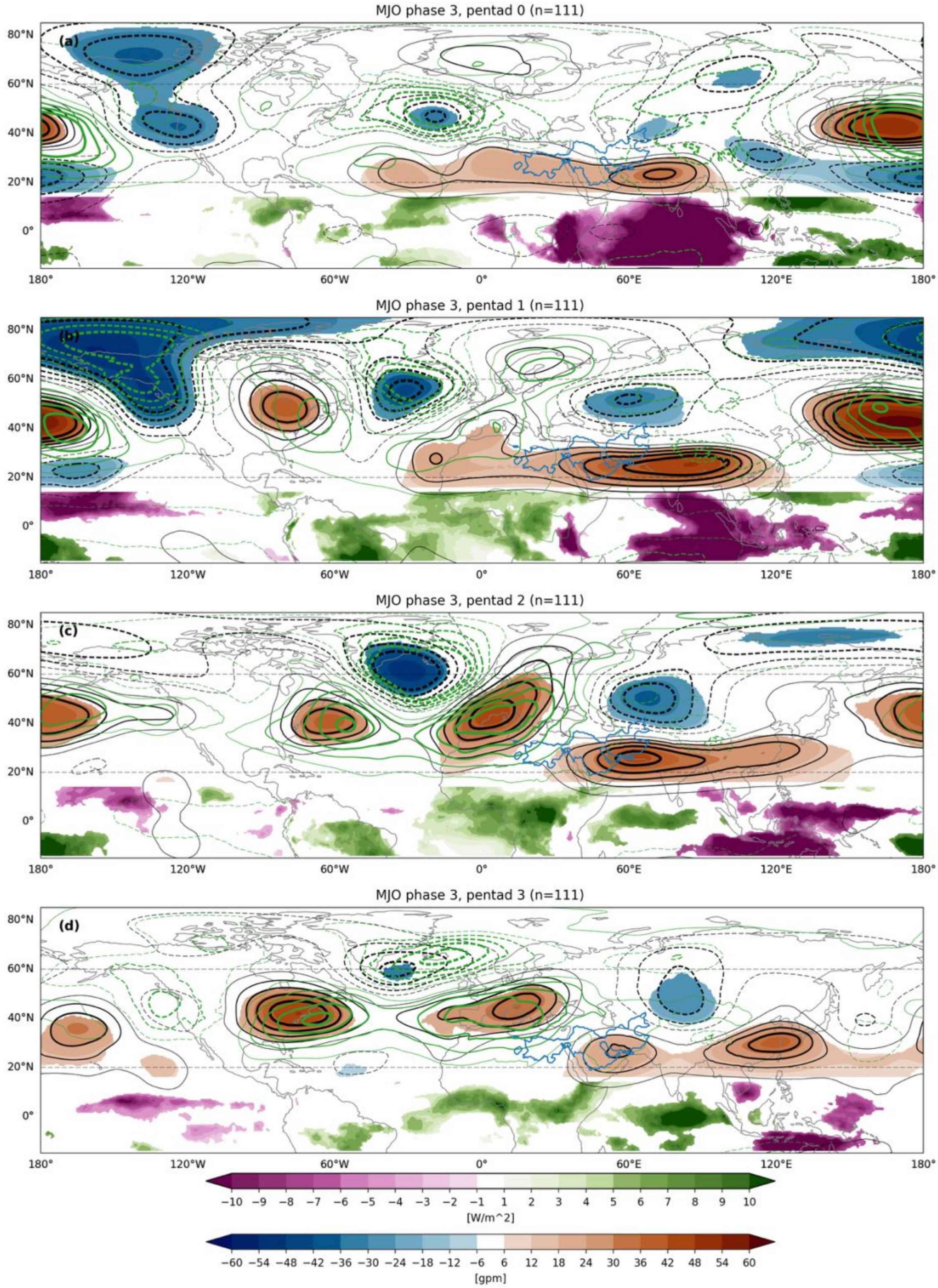

Figure 11. As Fig. 10 but for MJO events in phase 3.

https://doi.org/10.5194/egusphere-2026-5324
Preprint. Discussion started: 9 September 2026

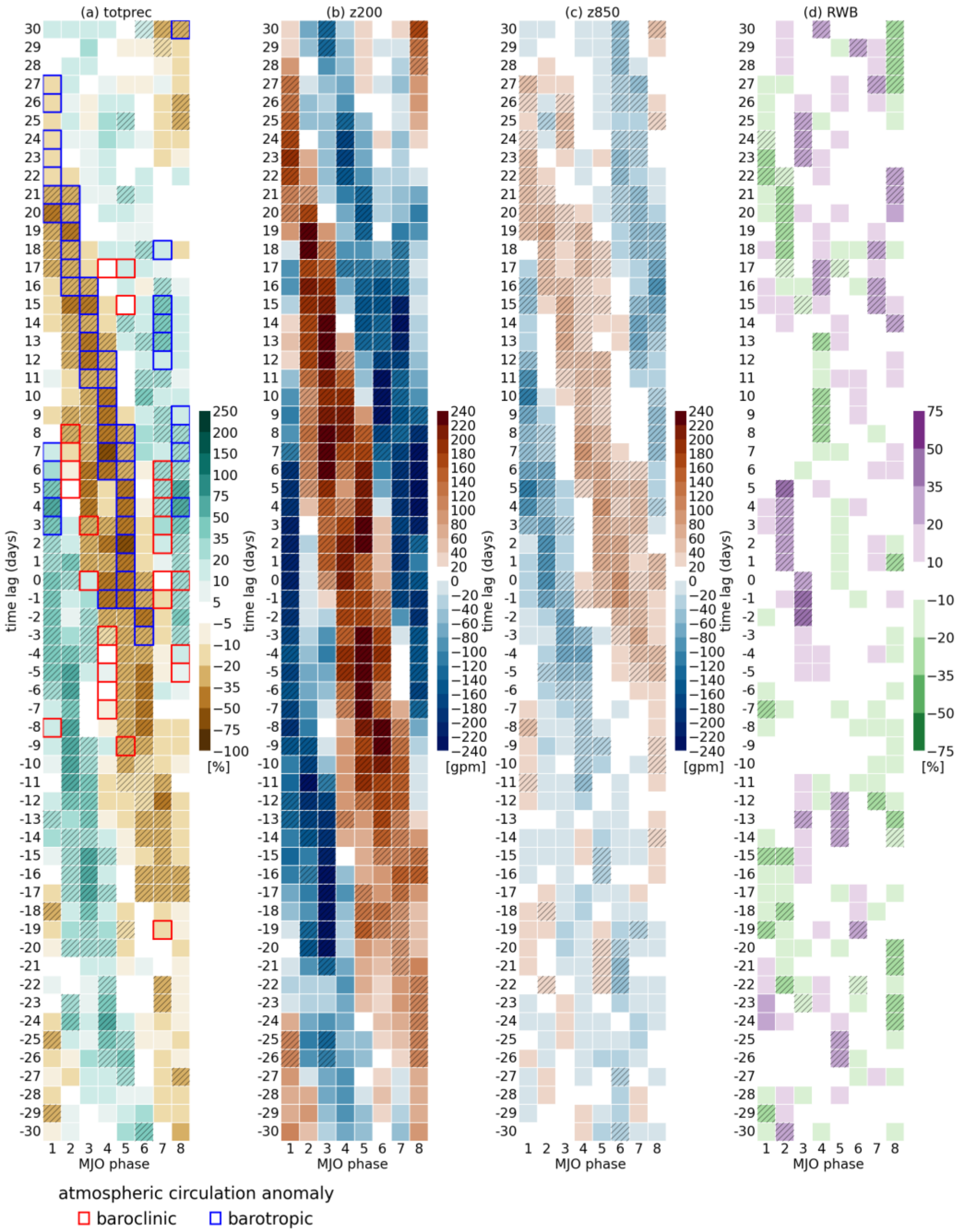

680 **Figure 12. Spatially averaged anomalies as a function of MJO phase and time lag (days) from MJO event onset showing (a) relative anomalies in precipitation over the target region, as in Fig. 5a, but with red and blue boxes indicating baroclinic and barotropic circulation anomalies based on opposed and equal signed anomalies, respectively, of 200-hPa and 850-hPa geopotential height. (b-d) spatially averaged anomalies over the region 35-55°E, 20-35°N, of (b) 250-hPa geopotential height, (c) 850-hPa geopotential height, and (d) vertically aggregated stratospheric PV structure occurrences. Hatching denotes statistical significance of anomalies at the p < 0.1 level.**

https://doi.org/10.5194/egusphere-2026-5324
Preprint. Discussion started: 9 September 2026

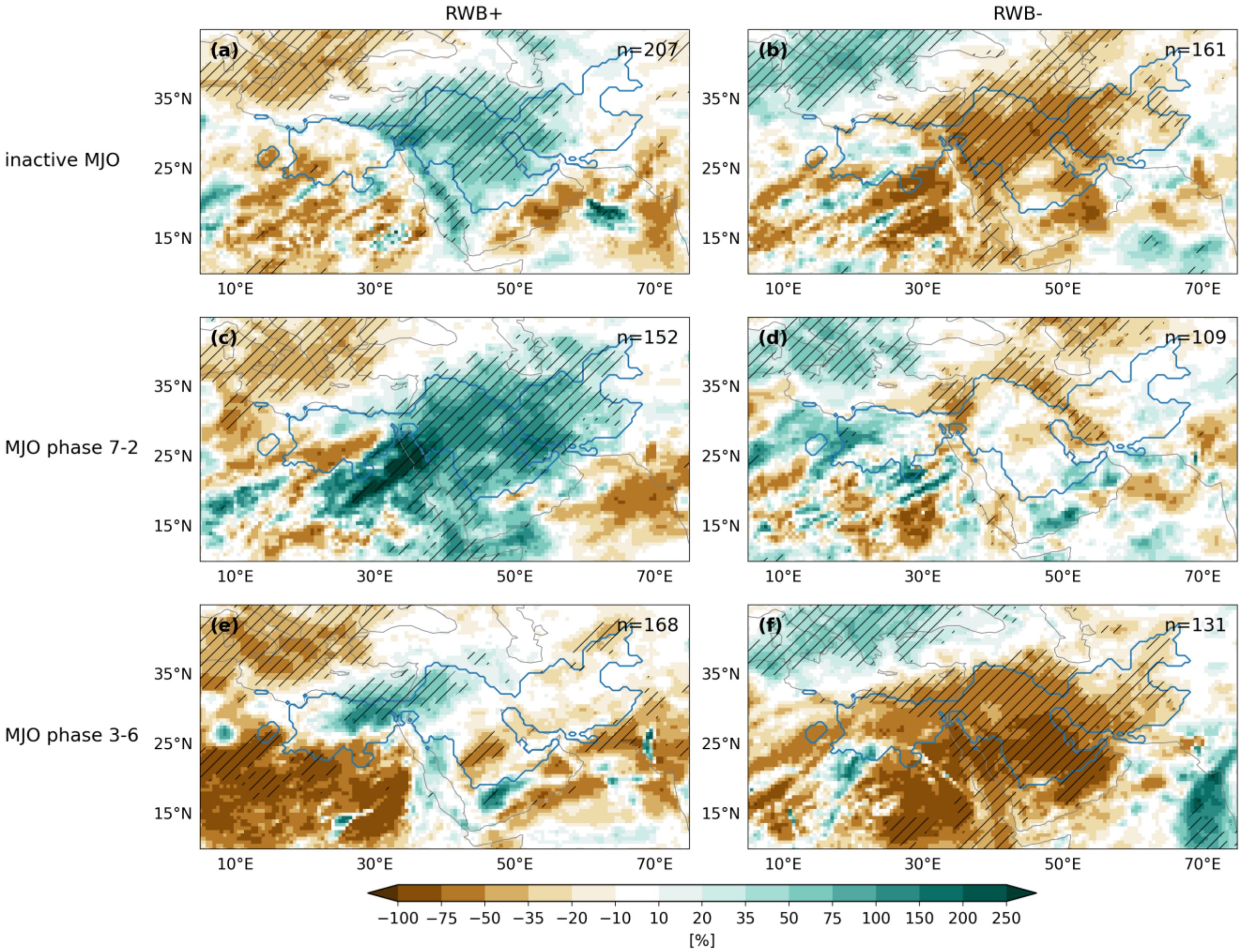

685 **Figure 13. Relative anomalies in multi-day precipitation from lag day -1 to +2 for events with RWB occurrence anomalies (a,c,e) exceeding 1 standard deviation from climatology and (b,d,f) falling below -1 standard deviation from climatology, concurring with (a,b) an inactive MJO, (c,d) MJO phases 7-2, and (e,f) MJO phases 3-6. Diagonal hatching denotes statistical significance in 4-day anomalies at the $p < 0.05$ level. The target region is for reference indicated in blue contours.**

https://doi.org/10.5194/egusphere-2026-5324
Preprint. Discussion started: 9 September 2026

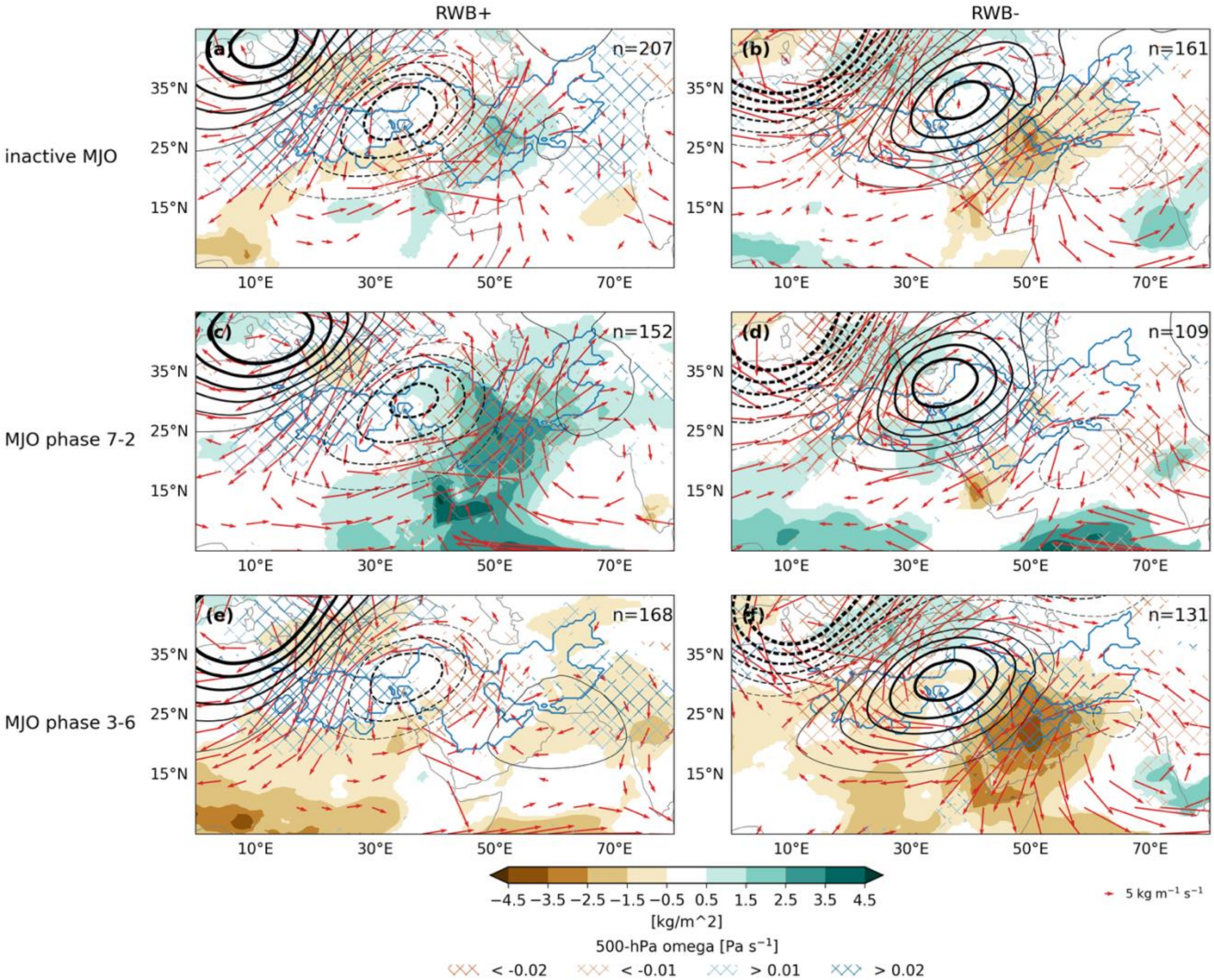

Figure 14. As Fig. 13 but then for anomalies in total column water (kg m^{-2}) in colors, only shown where statistically significant at the $p < 0.05$ level, in 500-hPa geopotential height contours at 4 gpm intervals up to 20 gpm with positive and negative values in solid and dashed, respectively, and in vertically integrated horizontal water vapor transport (kg m^{-1} s^{-1}) in red vectors where magnitudes of zonal and meridional component anomalies exceed 5 kg m^{-1} s^{-1}.

https://doi.org/10.5194/egusphere-2026-5324
Preprint. Discussion started: 9 September 2026

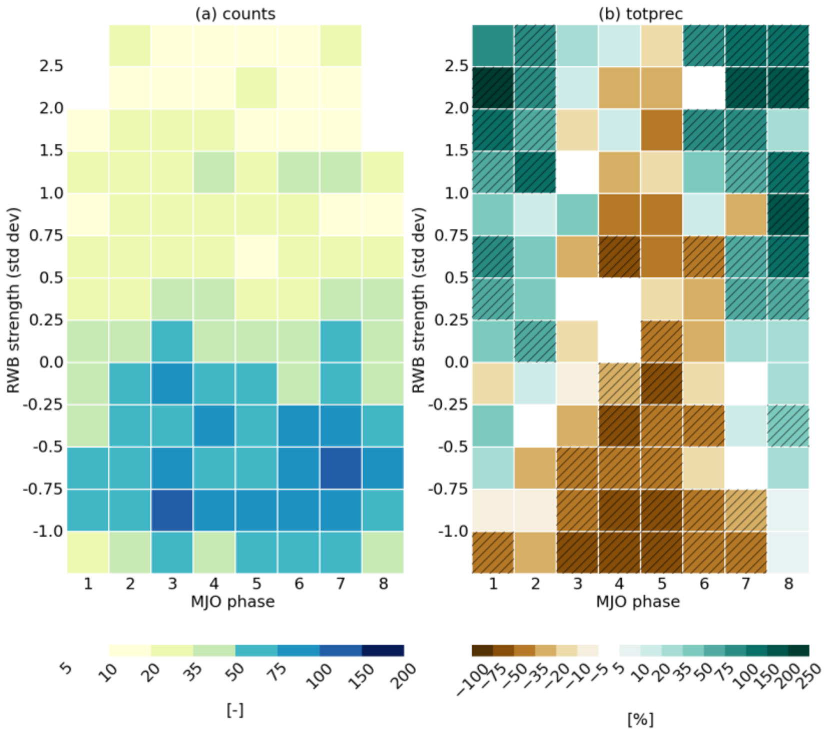

Figure 15. Heatmaps with (a) averaged number of days and (b) spatially averaged relative anomalies in precipitation (%) of days with anomalous RWB and concurring MJO phase. The data is based on binning RWB occurrence anomalies in the box 25-45E, 20-40N, also used to define anomalous RWB events (see Fig. 9a,k), and spatially aggregated precipitation in the target region. Hatching denotes statistical significance at the p < 0.1 level.

https://doi.org/10.5194/egusphere-2026-5324
Preprint. Discussion started: 9 September 2026

Appendix A

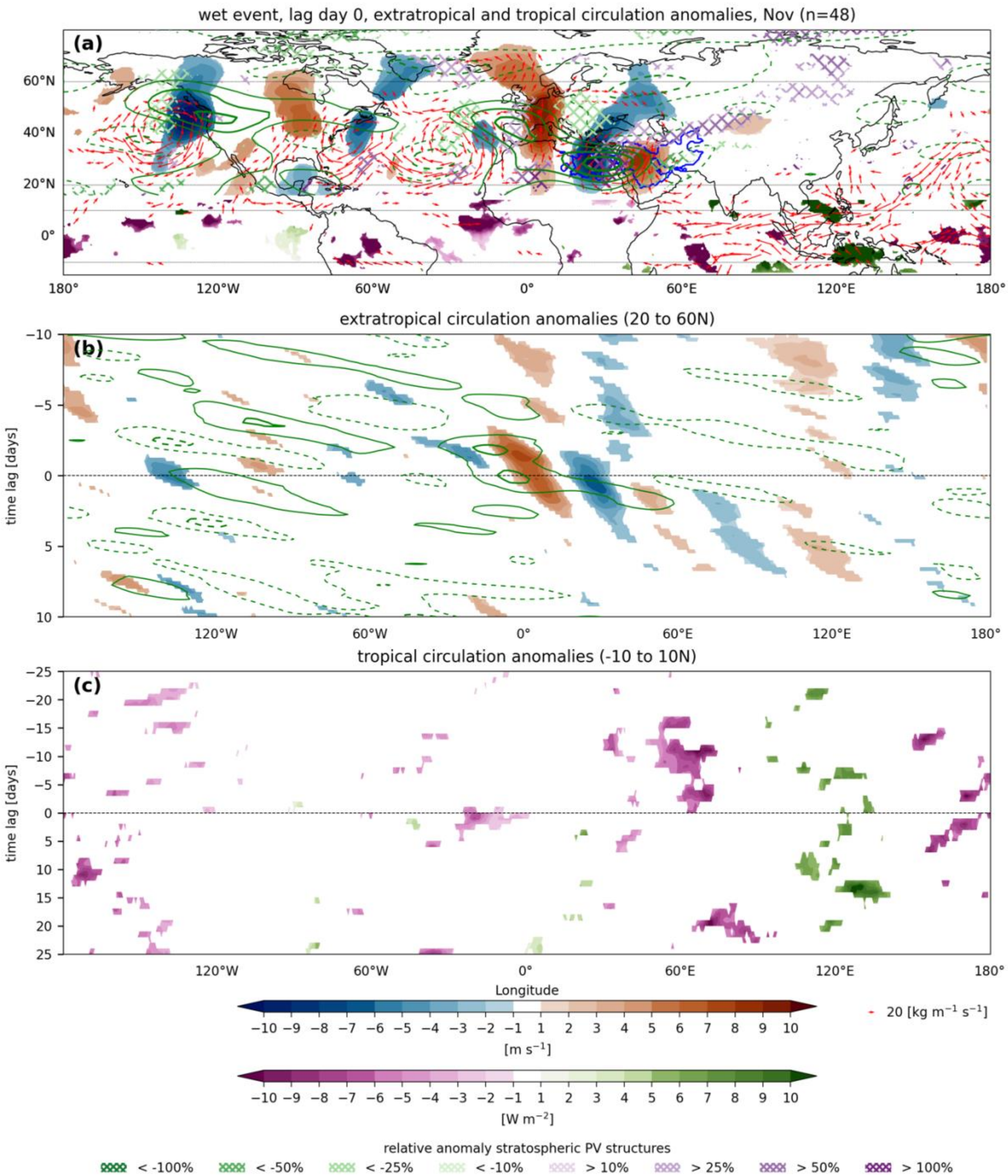

Figure A1. As Fig. 2 but for the month November and a two-sided test at the $p < 0.1$ level.

https://doi.org/10.5194/egusphere-2026-5324
Preprint. Discussion started: 9 September 2026

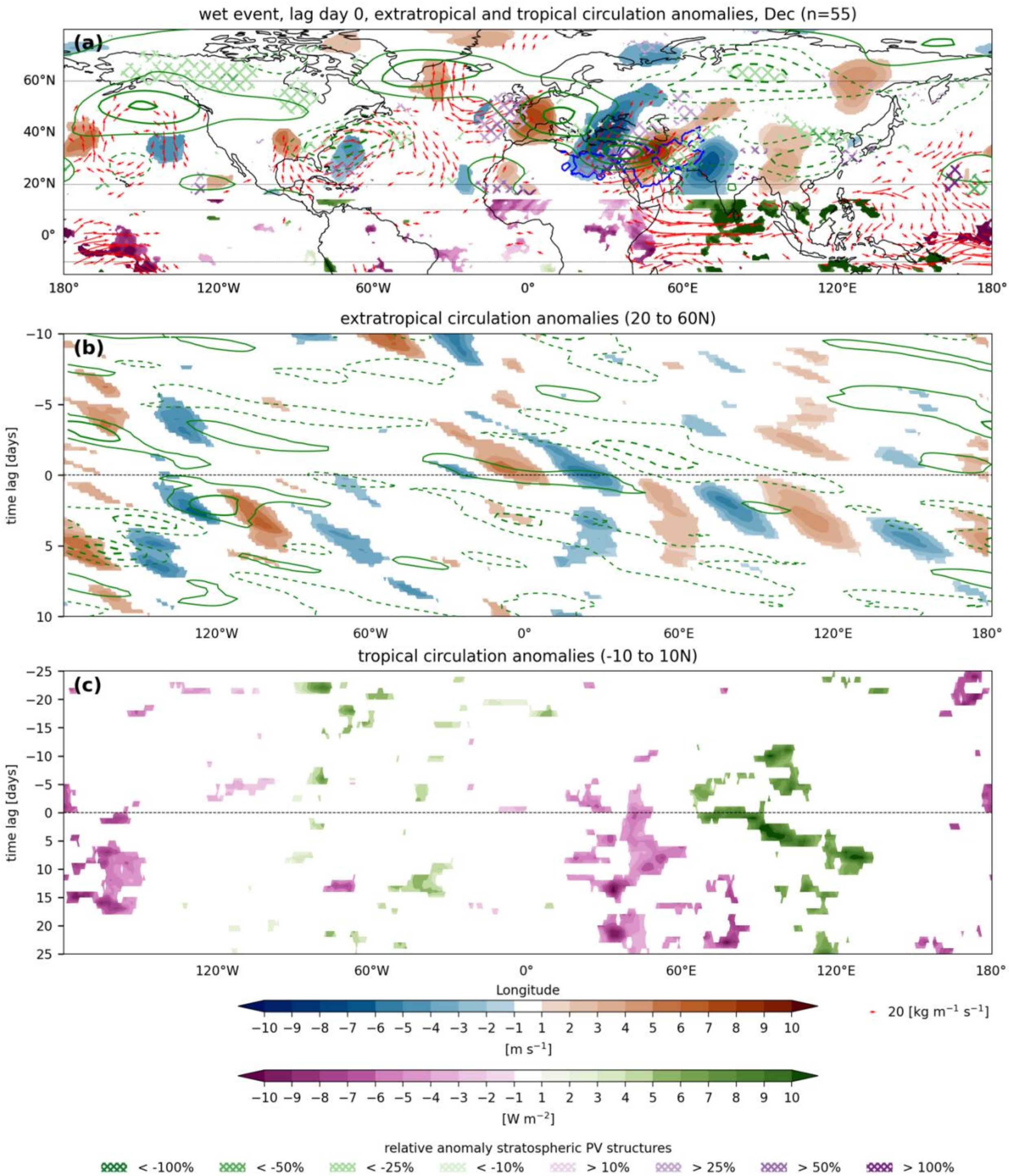

Figure A2. As Fig. 2 but for the month December and a two-sided test at the p < 0.1 level.

https://doi.org/10.5194/egusphere-2026-5324
Preprint. Discussion started: 9 September 2026

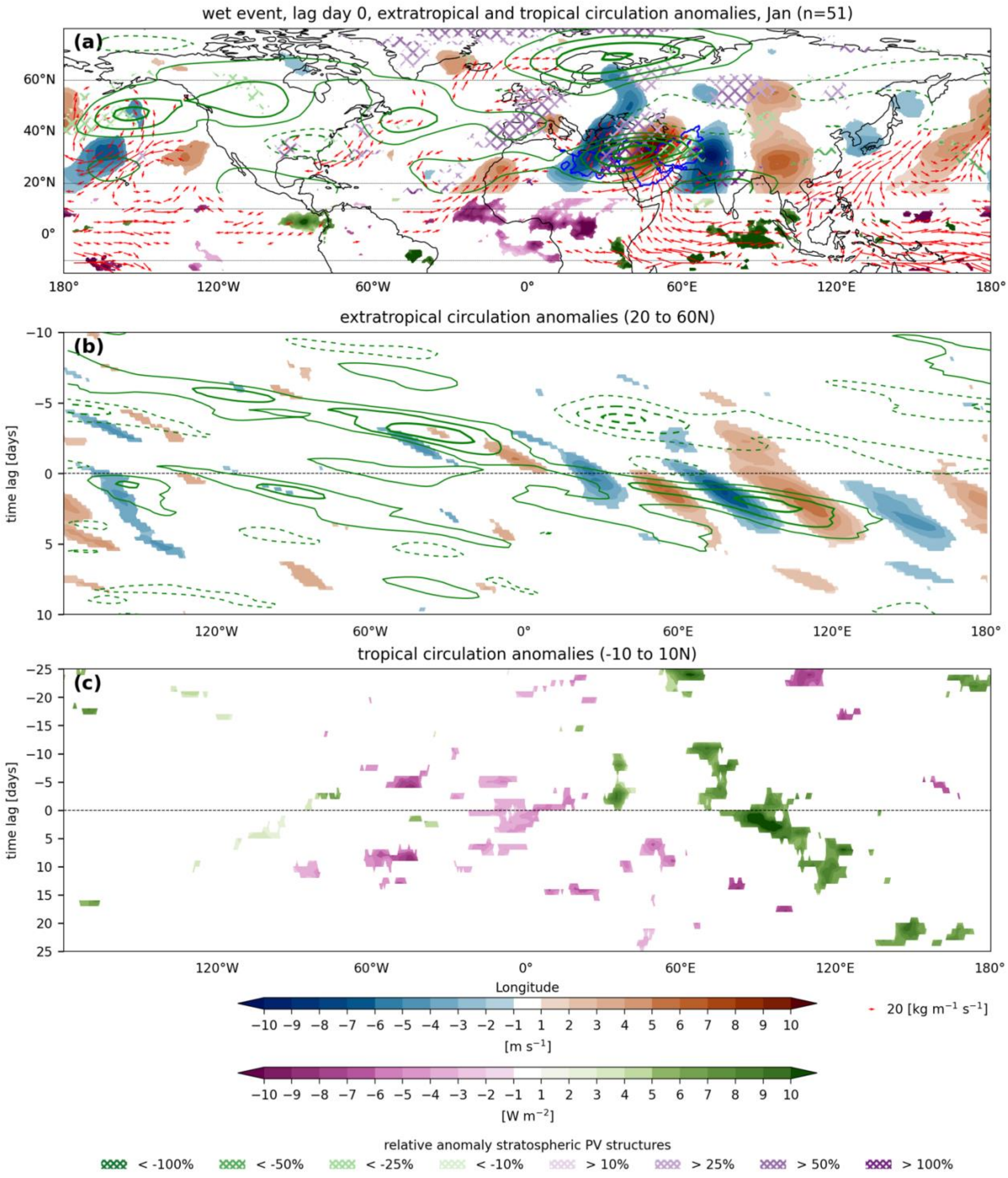

Figure A3. As Fig. 2 but for the month January and a two-sided test at the $p < 0.1$ level.

https://doi.org/10.5194/egusphere-2026-5324
Preprint. Discussion started: 9 September 2026

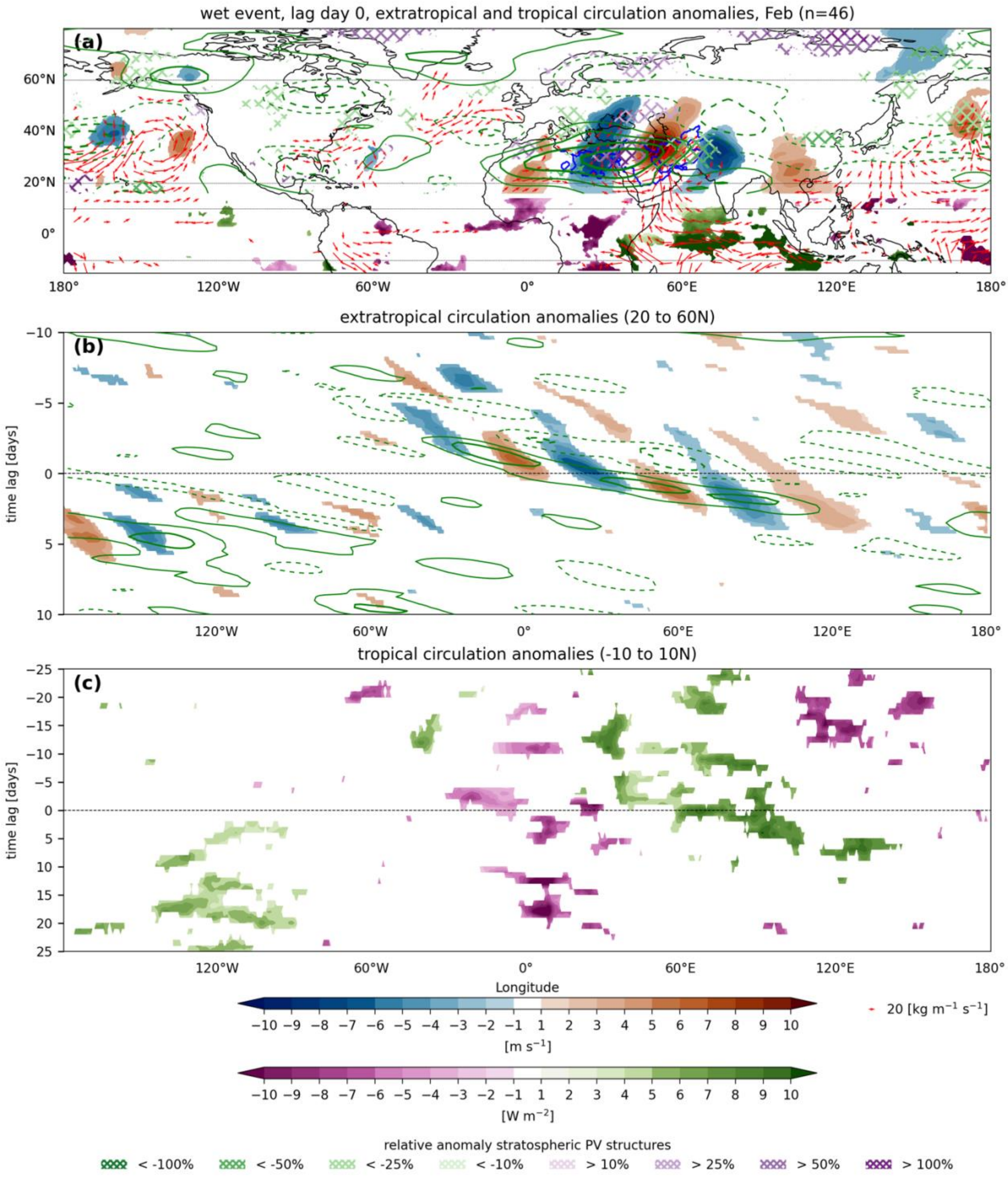

705 **Figure A4. As Fig. 2 but for the month February and a two-sided test at the p < 0.1 level.**

https://doi.org/10.5194/egusphere-2026-5324
Preprint. Discussion started: 9 September 2026

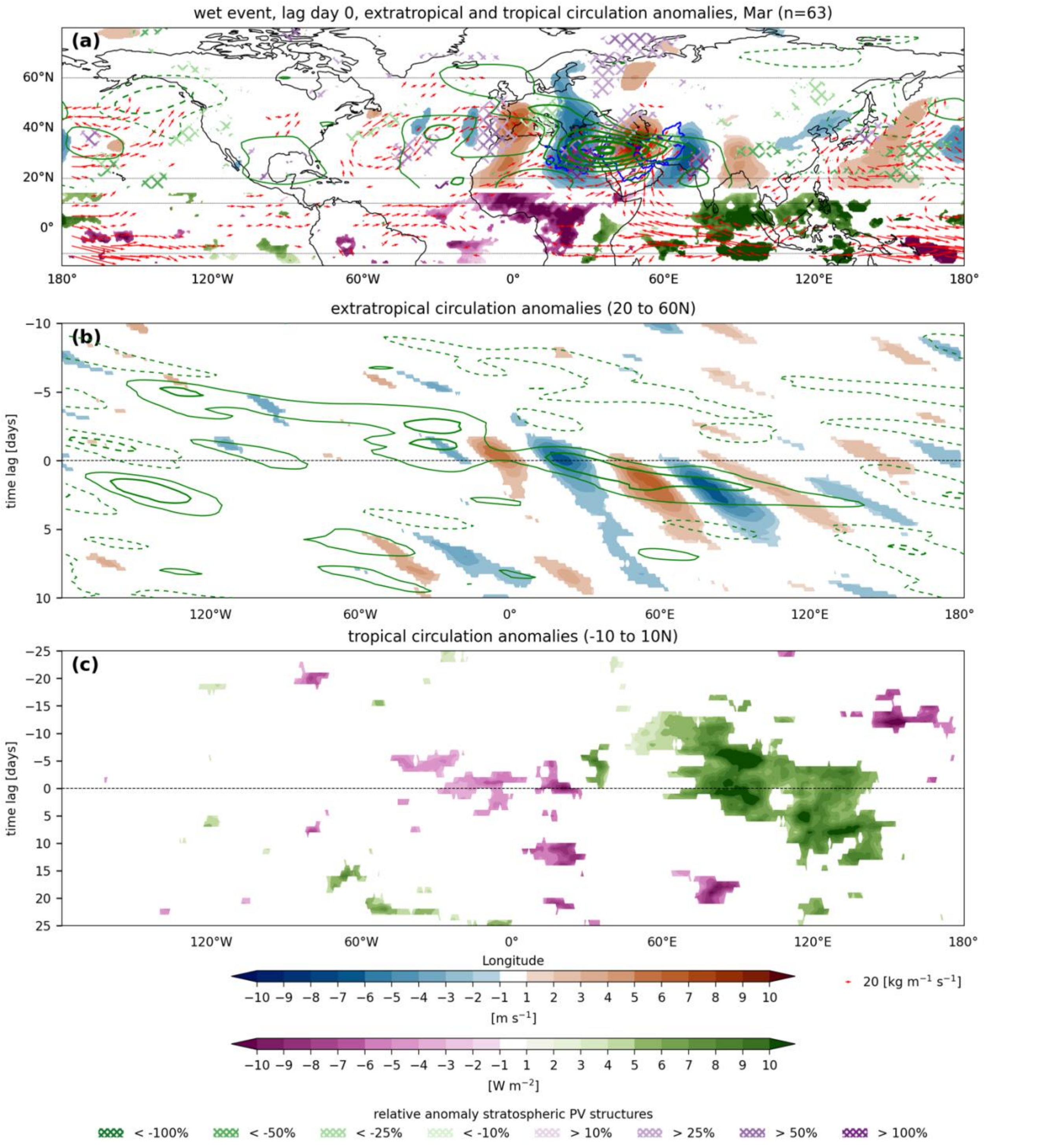

Figure A5. As Fig. 2 but for the month March and a two-sided test at the p < 0.1 level.

https://doi.org/10.5194/egusphere-2026-5324
Preprint. Discussion started: 9 September 2026

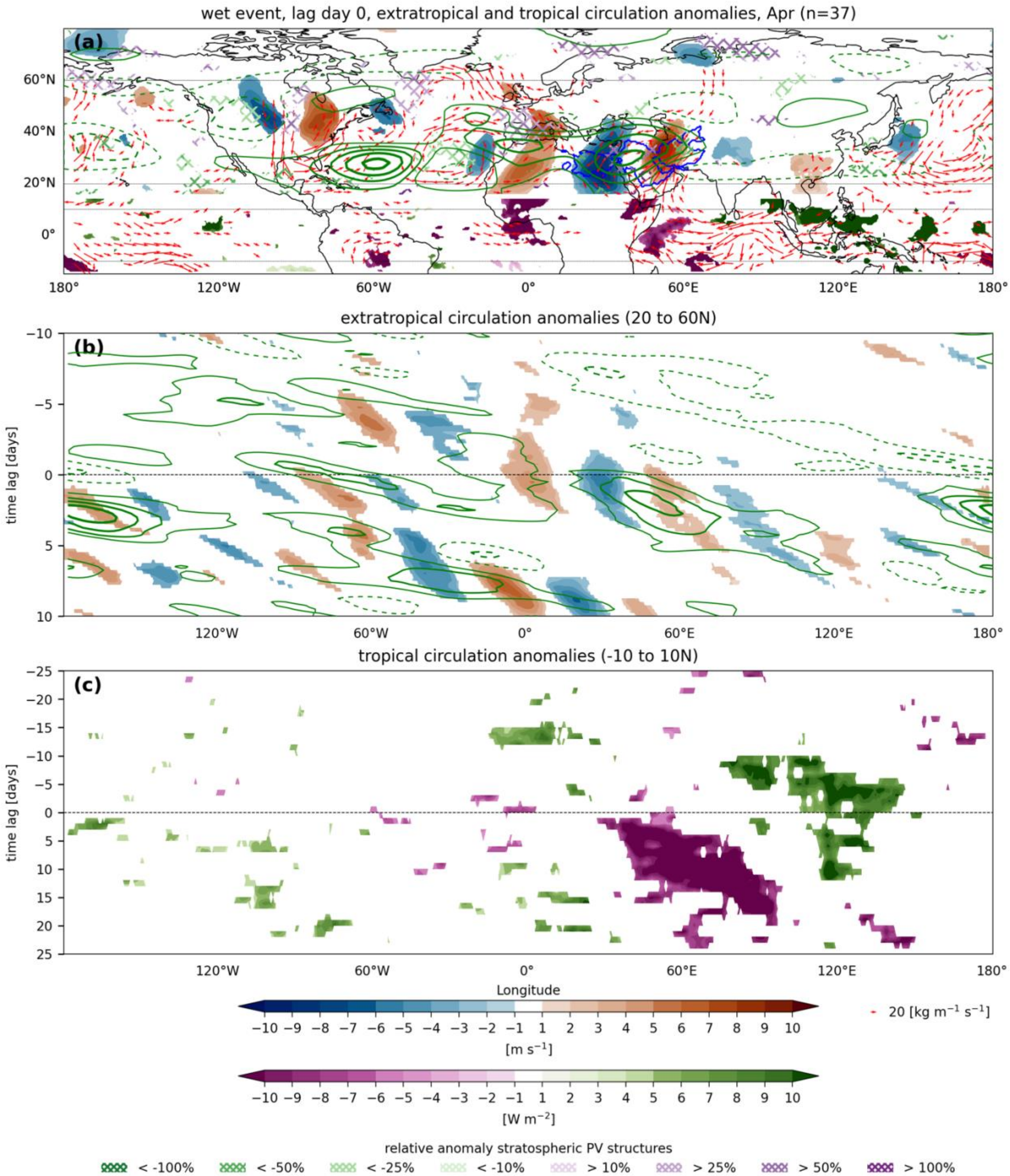

Figure A6. As Fig. 2 but for the month April and a two-sided test at the p < 0.1 level.

https://doi.org/10.5194/egusphere-2026-5324
Preprint. Discussion started: 9 September 2026

Code and data availability

All datasets used in this study are freely available from respective data providers. ERA5 data from the ECMWF was downloaded from the MARS archive and is also available from the Climate Data Store (https://cds.climate.copernicus.eu/). MSWEP from GloH2O was retrieved from the web (https://www.gloh2o.org). The RMM index was obtained from the Bureau of Meteorology (https://www.bom.gov.au/climate/mjo/).

Author contributions

AJV developed the idea for this study. AJV and GF provided data used in this study. AJV analysed and visualized the data used in this study and SFB contributed to the analysis and interpretation of the results. AJV wrote the initial draft of this manuscript. All authors contributed to reviewing and editing of the manuscript.

Competing interests

At least one of the (co-)authors is a member of the editorial board of Weather and Climate Dynamics.

Acknowledgements

AJV acknowledges the HPC DCSR from the University of Lausanne facilitating all computations performed in this study. The author has used AI for minor text corrections and for code debugging and minor code suggestions for processing and visualizing the data.

Financial support

D.D. acknowledges support from the Swiss National Science Foundation through project PP00P2_198896.

References

Abbas, M., Carling, P. A., Janse, J. D., Al-Saqarat, B. S.: Flash-flood hydrology and aquifer-recharge in Wadi Umm Sidr, Eastern Desert, Egypt, J. Arid Env., 178, 104170, https://doi.org/10.1016/j.jaridenv.2020.104170, 2020.

Ali, S. M., Martius, O., and Röthlisberger, M.: Recurrent Rossby wave packets modulate the persistence of dry and wet spells across the globe, Geophys. Res. Lett., 48, e2020GL091452, https://doi.org/10.1029/2020GL091452, 2021.

https://doi.org/10.5194/egusphere-2026-5324
Preprint. Discussion started: 9 September 2026

Alizadeh, Z. Mohebalhojeh, A. R., Ahmadi-Givi, F., Mirzaei, M., Khansalari, S.: The climatological impact of the upper-tropospheric Rossby wave propagation on the Red Sea trough in winter, Atmos. Res., https://doi.org/10.1016/j.atmosres.2020.105368, 2021.

Alizadeh, O., and Mousavizadeh, M.: Impact of ENSO on extreme precipitation in Southwest Asia, Glob. Plan. Change, 244, 104645, https://doi.org/10.1016/j.gloplacha.2024.104645, 2025.

Almazroui, M.: The influence of the Madden-Julian Oscillation on the west season rainfall over Saudi Arabia, Earth Syst. Env., 7, 1-14, https://link.springer.com/article/10.1007/s41748-022-00334-w, 2023.

Almazroui, M., Kamil, S., Ammar, K., Keay, K., Alamoudi, A.O.: Climatology of the 500-hPa mediterranean storms associated with Saudi Arabia wet season precipitation, Clim. Dyn., 47, 3029-3042, https://link.springer.com/article/10.1007/s00382-016-3011-0, 2016.

Almazroui, M. and Saeed, S.: Contribution of extreme daily precipitation to total rainfall over the Arabian Peninsula, Atmos. Res., 231, 104672, https://doi.org/10.1016/j.atmosres.2019.104672, 2020.

Armon, A., Dente, E., Smith, J. A., Enzel, Y., and Morin, E.: Synoptic-scale control over modern rainfall and flood patterns in the Levant drylands with implications for past climate, J. Hydrometeorol., 19, 1077-1096, https://doi.org/10.1175/JHM-D-18-0013.1, 2018.

Atif, R. M., Almazroui, M., Saeed, S., Abid, M. A., Islam, M. N. and Ismail, M.: Extreme precipitation events over Saudi Arabia during the wet season and their associated teleconnections, Atmos. Res., 231, 104655, https://doi.org/10.1016/j.atmosres.2019.104655, 2020.

Barlow, M., Wheeler, M., Lyon, B., and Cullen, H.: Modulation of daily precipitation over southwest Asia by the Madden-Julian Oscillation, Mon. Weath, Rev., 3579-3594, https://doi.org/10.1175/MWR3026.1, 2005.

Barlow, M., Hoell, A., and Colby, F.: Examining the wintertime response to tropical convection over the Indian Ocean by modifying convective heating in a full atmospheric model, Geophys. Res. Lett, 34, L19702, https://doi.org/10.1029/2007GL030043, 2007.

Barlow, M., Zaitchik, B., Paz, S., Black, E., Evans, J., and Hoell, A.: A Review of Drought in the Middle East and Southwest Asia, J. Climate, 29, 8547–8574, https://doi.org/10.1175/JCLI-D-13-00692.1, 2016.

Beck, H. E., Wood, E. F., Pan, M., Fisher, C. K., Miralles, D. G., van Dijk, A. I., McVicar, T. R., and Adler, R. F.: MSWEP V2 global 3-hourly 0.1 precipitation: methodology and quantitative assessment, B. Am. Meteorol. Soc., 100, 473–500, https://doi.org/10.1175/BAMS-D-17-0138.1, 2019.

Berkovic, S. and Raveh-Rubin, S.: Persistent warm and dry extremes over the eastern Mediterranean during winter: The role of North Atlantic blocking and central Mediterranean cyclones, Q. J. Roy. Meteorol. Soc., 148, 2384–2409, https://doi.org/10.1002/qj.4308, 2022.

Breeden, M. L., Albers, J. R., and Hoell, A.: Subseasonal precipitation forecasts of opportunity over central southwest Asia, Weather Clim. Dynam., 3, 1183–1197, https://doi.org/10.5194/wcd-3-1183-2022, 2022.

Cannon, F., Carvalho, L. M. V., Jones, C., Hoell, A., Norris, J., Kiladis, G. N., and Tahir, A. A.: The influence of tropical forcing on extreme winter precipitation in the western Himalaya, Clim. Dynam., 48, 1213–1232, https://doi.org/10.1007/s00382-016-3137-0, 2017.

Chenoweth, J., Hadjinicolaou, P., Bruggeman, A., Lelieveld, J., Levin, Z., Lange, M. A., Xoplaki, E. and Hadjikakou, M.: Impact of climate change on the water resources of the eastern Mediterranean and Middle East region: Modeled 21st century changes and implications, Water Resources Res., 47, W06506, https://doi.org/10.1029/2010WR010269, 2011.

Coleman, M., de Vries, A. J., Roberts, C., and Domeisen, D.I.V.: Floods in the European Union and the Middle East and North Africa region: Socio-economic impacts, characteristics, and perception, under review in Nat. Haz. Earth Syst. Env, https://egusphere.copernicus.org/preprints/2026/egusphere-2026-1827/.

Daoudry, M, Sowers, J. and Weinthal, E.: What is climate security? Framing risks around water, food, and migration in the Middle East and North Africa, WIREs water, e1582, https://doi.org/10.1002/wat2.1582, 2022.

de Vries, A. J., Tyrlis, E., Edry, D., Krichak, S. O., Steil, B., and Lelieveld, J.: Extreme precipitation events in the Middle East: Dynamics of the Active Red Sea Trough, J. Geophys. Res.-Atmos., 118, 7087–7108, https://doi.org/10.1002/jgrd.50569, 2013.

de Vries, A. J., Feldstein, S. B., Riemer, M., Tyrlis, E., Sprenger, M., Baumgart, M., Fnais, M., and Lelieveld, J.: Dynamics of tropical-extratropical interactions and extreme precipitation events in Saudi Arabia in autumn, winter and spring, Q. J. Roy. Meteor. Soc., 142, 1862–1880, https://doi.org/10.1002/qj.2781, 2016.

https://doi.org/10.5194/egusphere-2026-5324
Preprint. Discussion started: 9 September 2026

de Vries, A. J., Ouwersloot, H. G., Feldstein, S. B., Riemer, M., El Kenawy, A. M., McCabe, M. F., and Lelieveld, J.: Identification of tropical-extratropical interactions and extreme precipitation events in the Middle East based on potential vorticity and moisture transport, J. Geophys. Res.-Atmos., 123, 861–881, https://doi.org/10.1002/2017JD027587, 2018.

de Vries, A. J., Armon, M., Klingmüller, K., Portmann, R., Röthlisberger, M., Domeisen, D. I. V.: Breaking Rossby waves drive extreme precipitation in the world's arid regions, Commun. Earth & Env., 5, 493, https://www.nature.com/articles/s43247-024-01633-y, 2024.

de Vries, A. J.: A global climatological perspective on the importance of Rossby wave breaking and intense moisture transport for extreme precipitation events, Weather Clim. Dynam., 2, 129–161, https://doi.org/10.5194/wcd-2-129-2021, 2021.

de Vries, A.-J., Feldstein, S. B., Casselman, J. W., Fragkoulidis, G., Lelieveld, J., and Domeisen, D. I. V.: The influence of El Niño-Southern Oscillation on cool-season precipitation variability in the arid Middle East, Weath. Clim. Dynam, 7, 1479-1505, https://doi.org/10.5194/wcd-7-1479-2026, 2026.

ESCWA, Demographic trends in the Arab region: 1950-2030, United Nations, , https://www.unescwa.org/publications/demographic-trends-arab-region-1950-2030, 2025.

Evans, J. and Smith, R.: Water vapor transport and the production of precipitation in the eastern Fertile Crescent, J. Hydrometeorol., 7, 1295–1307, https://doi.org/10.1175/JHM550.1, 2006.

Feldstein, S. B. and Dayan, U.: Circumglobal teleconnections and wave packets associated with Israeli winter precipitation, Q. J. Roy. Meteorol. Soc., , 134, 455–467, https://doi.org/10.1002/qj.225, 2008.

Fragkoulidis, G.: Decadal variability and trends in extratropical Rossby wave packet amplitude, phase, and phase speed, Weather Clim. Dynam., 3, 1381–1398, https://doi.org/10.5194/wcd-3-1381-2022, 2022.

Francis, D., Fonseca, R., Nelli, N., Cherif, C., Yarragunta, Y., Zittis, G., and de Vries, A. J.: From cause to consequence: examining the historic April 2024 rainstorm in the United Arab Emirates through the lens of climate change, npj Clim.Atmos. Sci., 8, 183, https://www.nature.com/articles/s41612-025-01073-1, 2025.

Ghassabi, Z., Fattahi, E. and Habibi, M.: Daily atmospheric circulation patterns and their influence on dry/wet events in Iran, Atmos., 13, 81, https://doi.org/10.3390/atmos13010081, 2021.

https://doi.org/10.5194/egusphere-2026-5324
Preprint. Discussion started: 9 September 2026

Gill, A. E.: Some simple solutions for heat-induced tropical circulation, Q. J. Roy. Meteor. Soc., 106, 447-462, https://doi.org/10.1002/qj.49710644905, 1980.

Gleick, P. H.: Water, drought, climate change, and conflict in Syria, Weather Clim. Soc. 6, 331–340, https://doi.org/10.1175/WCAS-D-13-00059.1, 2014.

Govardhan, D., Pathak, R., Ashok, K., Asiri, M. I. Zamreeq, A., Hoteit, I.: Midlatitude circulations linked to seasonal extreme precipitation and extreme temperature events in the Arabian Peninsula, Clim. Dyn., 63, https://link.springer.com/article/10.1007/s00382-025-07592-0, 2025.

Grazzini, F., Fragkoulidis, G., Teubler, F., Wirth, V., Craig, G. C.: Extreme precipitation events over northern Italy. Part II: Dynamical precursors, Q. J. Roy. Meteor. Soc., 147, 1237-1257, https://doi.org/10.1002/qj.3969, 2021.

Guo, Y., Shinoda, T., Lin, J., and Chang, E. K.: Variations of Northern Hemisphere storm track and extratropical cyclone activity associated with the Madden-Julian oscillation, J. Climate, 30, 4799–4818, https://doi.org/10.1175/JCLI-D-16-0513.1, 2017.

Haris, I., Osborn, T. J., Jones, P. and Lister, D.: Version 4 of the CRU TS monthly high-resolution gridded multivariate climate datasets. Sci. Data, 7, 109, https://www.nature.com/articles/s41597-020-0453-3, 2020.

Hendon, H. H., Zhang, C., and Glick, J. D.: Interannual variation of the Madden-Julian Oscillation during Austral summer, J. Climate, 12, 2538-2550, https://doi.org/10.1175/1520-0442(1999)012%3C2538:IVOTMJ%3E2.0.CO;2, 1999.

Hersbach, H., Bell, B., Berrisford, P., Hirahara, S., Horányi, A., Muñoz-Sabater, J., Nicolas, J., Peubey, C., Radu, R., Schepers, D., Simmons, A., Soci, C., Abdalla, S., Abellan, X., Balsamo, G., Bechtold, P., Biavati, G., Bidlot, J., Bonavita, M., De Chiara, G., Dahlgren, P., Dee, D., Diamantakis, M., Dragani, R., Flemming, J., Forbes, R., Fuentes, M., Geer, A., Haimberger, L., Healy, S., Hogan, R. J., Hólm, E., Janisková, M., Keeley, S., Laloyaux, P., Lopez, P., Lupu, C., Radnoti, G., de Rosnay, P., Rozum, I., Vamborg, F., Villaume, S., and Thépaut, J.-N.: The ERA5 global reanalysis, Q. J. Roy. Meteor. Soc., 146, 1999–2049, https://doi.org/10.1002/qj.3803, 2020.

Hochman, A., Marra, F., Messori, G., Pinto, J. G., Raveh-Rubin, S., Yosef, Y., and Zittis, G.: Extreme weather and societal impacts in the eastern Mediterranean, Earth Syst. Dynam., 13, 749–777, https://doi.org/10.5194/esd-13-749-2022, 2022.

https://doi.org/10.5194/egusphere-2026-5324
Preprint. Discussion started: 9 September 2026

Hoell, A., Barlow, M., and Saini, R.: The leading pattern of intraseasonal and interannual Indian Ocean precipitation variability and its relationship with Asian circulation during the boreal cold season, J. Climate, 25, 7509–7526, https://doi.org/10.1175/JCLI-D-11-00572.1, 2012.

Hoell, A., Barlow, M., and Saini, R.: Intraseasonal and seasonal-to-interannual Indian Ocean convection and hemispheric teleconnections, J. Climate, 26, 8850–8867, https://doi.org/10.1175/JCLI-D-12-00306.1, 2013.

Hoell, A., Cannon, F., and Barlow, M.: Middle East and Southwest Asia Daily Precipitation Characteristics Associated with the Madden–Julian Oscillation during Boreal Winter, J. Climate, 31, 8843–8860, https://doi.org/10.1175/JCLI-D-18-0059.1, 2018.

Hoell., A., Breeden, M., Worsnop, R. P., Robinson, R., Agel, L., Anderson, W., Barlow, M., Jayanthi, H., McNally, A., Shukla, S., Slinski K., Verdin, J., Zaheer, F.: An unexpected outcome followed an apparent seasonal forecast of opportunity and prolonged drought in southwest Asia, Int. J. Climatol., 45,8, e8861, https://doi.org/10.1002/joc.8851, 2025.

Hunt, K. M. R., Turner, A. G., and Shaffrey, L. C.: The evolution, seasonality, and impacts of western disturbances, *Quart. J. Roy. Meteor. Soc.*, 144, 278–290, https://doi.org/10.1002/qj.3200, 2018.

Kahana, R., Ziv, B., Enzel, Y., and Dayan, U.: Synoptic climatology of major floods in the Negev Desert, Israel, Int J. Climatol., 22, 867–882, https://doi.org/10.1002/joc.766, 2002.

Kelley, C. P., Mohtadi, S., Cane, M. A., Seager, R., and Kushnir, Y.: Climate change in the Fertile Crescent and implications of the recent Syrian drought. Proc. Natl Acad. Sci., 112, 3241–3246, https://doi.org/10.1073/pnas.1421533112, 2015.

Niranjan Kumar, K., D. Entekhabi, and Molini, A.: Hydrological extremes in hyperarid regions: A diagnostic characterization of intense precipitation over the Central Arabian Peninsula, J. Geophys. Res. Atmos., 120, 5, 1637–1650, https://doi.org/10.1002/2014JD022341, 2015.

Madden, R. A. and Julian, P. R.: Detection of a 40–50 Day Oscillation in the Zonal Wind in the Tropical Pacific, J. Atmos. Sci., 28, 702–708, https:// doi. org/ 10. 1175/ 1520-0469(1971) 028< 0702: DOADO I> 2.0.CO; 2., 1971.

Martius, O., Schwierz, C. and Davies, H. C.: Far-upstream precursors of heavy precipitation events on the Alpine south-side. *Quart. J. Roy. Meteor. Soc.*, **134**, 417–428, https://doi.org/10.1002/qj.229, 2008.

Matus, F., Rondanelli, R., Rutllant, J., and Henderson, S.: Mechanisms for the influence of the MJO on precipitation in Southwestern South America. Journal of Geophysical Research: Atmospheres, 130, e2024JD041935. https://doi.org/10.1029/2024JD041935, 2025.

Matsuno, T.: Quasi-geostrophic motions in the Equatorial Area, J. Meteor., Soc. Japan, 44, 25-43, https://doi.org/10.2151/jmsj1965.44.1_25, 1966.

Mundhenk, B. D., Barnes, E. A., and Maloney, E. D.: All-Season Climatology and Variability of Atmospheric River Frequencies over the North Pacific, J. Climate, 29, 4885–4903, https://doi.org/10.1175/JCLI-D-15-0655.1, 2016.

Nazemosadat, M. J. and Ghaedamini, H.: On the relationships between the Madden–Julian oscillation and precipitation variability in southern Iran and the Arabian Peninsula: Atmospheric circulation analysis, J. Climate, 23, 887–904, https://doi.org/10.1175/2009JCLI2141.1, 2010.

Nazemosadat, M. J and Shahgholian, K.: Heavy precipitation in the southwest of Iran: association with the Madden–Julian Oscillation and synoptic scale analysis, Clim. Dyn. 49:3091–3109, https://link.springer.com/article/10.1007/s00382-016-3496-6, 2017.

Nelli, N. R., Francis, D., Fonseca, R., Abida, R., Weston, M., Wehbe, Y., and Al Hosary, T.: The atmospheric controls of extreme convective events over the southern Arabian Peninsula during the spring season, Atm. Res., 262, 105788, https://doi.org/10.1016/j.atmosres.2021.105788, 2021.

Oikonomo, C., Flocas, H. A., Hatzaki, M., Nisantzi, A., Asimakopoulos, D. N.: Relationship of extreme dry spells in eastern Mediterranean with large-scale circulation, Theor. Appl., Climatol., 100:137=151, https://link.springer.com/article/10.1007/s00704-009-0171-4, 2010.

Pohl, B. and Matthews, A. J.: Observed changes in the lifetime and amplitude of the Madden–Julian oscillation associated with interannual ENSO sea surface temperature anomalies, J. Climate, 20, 2659–2674, https://doi.org/10.1175/jcli4230.1, 2007.

Portmann, R., Sprenger, M. and Wernli, H.: The three-dimensional life cycles of potential vorticity cutoffs: a global and selected regional climatologies in ERA-Interim (1979-2018). *Wea. Clim. Dyn.*, 2, 507-534, https://doi.org/10.5194/wcd-2-507-2021, 2021.

https://doi.org/10.5194/egusphere-2026-5324
Preprint. Discussion started: 9 September 2026

Pourasghar, F., Tozuka, T., Ghaemi, H. oettli, P., Jahanbakhsh, S., and Yamagata, T.: Influences of the MJO on intraseasonal rainfall variability over Southern Iran, Atmos. Sci. Lett., 16, 110-118, https://doi.org/10.1002/asl2.531, 2015.

Pourasghar, F., Oliver, E. C. J., Holbrook, N. J.: Modulation of wet-season rainfall over Iran by the Madden-Julian Oscillation, Indian Ocean Dipole, and El Niño-Southern Oscillation, Int. J. Climatol., 39, 4029-4040, doi.org/10.1002/joc.6057, 2019.

Quinting, J. F., Grams, C. M., Chang, E. K.-M., Pfahl, S., and Wernli, H.: Warm conveyor belt activity over the Pacific: modulation by the Madden–Julian Oscillation and impact on tropical–extratropical teleconnections, Weather Clim. Dynam., 5, 65–85, https://doi.org/10.5194/wcd-5-65-2024, 2024.

Raoufi, A. and Tsubaki, K.: Reviving ancestral water management practices: A sustainable and resilient design approach addressing the flood-drought paradox in rural Ahvaz, Iran, J. Env. Management, 385, 125476, https://doi.org/10.1016/j.jenvman.2025.125476, 2025.

Raziei, T., Bordi, I., Pereira, L. S., Corte-Real, J., Santos, J. A.: Relationship between daily atmospheric circulation types and winter dry/wet spells in western Iran, Int. J. Climatol., 32, 1056-1068, https://doi.org/10.1002/joc.2330, 2012.

Rodwell, M. J. and Hoskins, B. J.: Monsoon and the dynamics of deserts. Quarterly Journal of the Royal Meteorological Society, 122, 1385–1404. https://doi.org/10.1002/qj.49712253408, 1996.

Rodwell, M. J. and Hoskins, B. J.: Subtropical anticyclones and summer monsoons, 14, 3192-3211, https://doi.org/10.1175/1520-0442(2001)014%3C3192:SAASM%3E2.0.CO;2, 2001.

Rubin, S., Ziv, B. and Paldor N.: Tropical plumes over eastern North Africa as a source of rain in the Middle East, Mon. Weath. Rev., 135: 4135–4148, https://doi.org/10.1175/2007MWR1919.1., 2007.

Saaroni, H., Halfon, N., Ziv, B., Alpert, P., and Kutiel, H.: Links between the rainfall regime in Israel and location and intensity of Cyprus lows, Int. J. Climatol., 30, 1014–1025, https://doi.org/10.1002/joc.1912, 2010.

Saaroni, H., Ziv, B., Lempert, J., Gazit, Y., and Morin, E.: Prolonged dry spells in the Levant region: climatologic-synoptic analysis, Int. J. Climatol., 35, 2223–2236, https://doi.org/10.1002/joc.4143, 2015.

Saaroni, H., Ziv, B., Harpaz, T., and Lempert, J.: Dry events in the winter in Israel and its linkage to synoptic and large-scale circulations, Int. J. Climatol., 39, 1054–1071, https://doi.org/10.1002/joc.5862, 2019.

https://doi.org/10.5194/egusphere-2026-5324
Preprint. Discussion started: 9 September 2026

Saeed, S. and Almazroui, M.: Impacts of mid-latitude circulation on winter precipitation over the Arabian Peninsula, Clim. Dyn., 53, 5253-5264, https://link.springer.com/article/10.1007/s00382-019-04862-6, 2019.

Sandler, D., Saaroni, H., Ziv, B., Tamarin-Brodsky, T., and Harnik, N.: The connection between North Atlantic storm track regimes and eastern Mediterranean cyclonic activity, Weath. Clim. Dynam., 5, 1103–1116, https://doi.org/10.5194/wcd-5-1103-2024, 2024.

Sherif, M., Sefelnasr, A., Al Rashed, M., Alshamsi, D., Zaidi, F. K., Alghafli, K., Baig, F., Al-Turbak, A., Alfaifi, H., Loni, O. A., Ahamed, M. B., and Ebraheem, A. A.: A Review of Managed Aquifer Recharge Potential in the Middle East and North Africa Region with Examples from the Kingdom of Saudi Arabia and the United Arab Emirates, Water, 15, https://doi.org/10.3390/w15040742, 2023.

Tippett, M., Almazroui, M. and Kang, I-S.: Extended-range forecasts of areal-averaged rainfall over Saudi Arabia, Wea. Forecast., 30, 1090-1105, https://doi.org/10.1175/WAF-D-15-0011.1, 2015.

Toride, K., Hakim, G. J., Hoell, A.: Roles of MJO and tropical-extratropical interactions in subseasonal conditions related to landfalling atmospheric rivers, J. Climate, 39, 885-901, https://doi.org/10.1175/JCLI-D-25-0211.1, 2026.

Tozer, C. R., Risbey, J. S., O'Kane, T. J., Monselesan D. P. and Pook, M. J.: The relationship between wave trains in the Southern Hemisphere storm track and refinall extremes over Tasmania, Mon. Weath. Rev, 146, 4201-4230, https://doi.org/10.1175/MWR-D-18-0135.1, 2018.

Tseng, K.-C., Maloney, E., and Barnes, E.: The Consistency of MJO Teleconnection Patterns: An Explanation Using Linear Rossby Wave Theory, J. Climate, 32, 531–548, https://doi.org/10.1175/JCLI-D-18-0211.1, 2019.

Tubi, A., Dayan, U., and Lensky, I. M.: Moisture transport by tropical plumes over the Middle East: a 30-year climatology, Q. J. Roy. Meteor. Soc., 143, 3165–3176, https://doi.org/10.1002/qj.3170, 2017.

Tuel, A., Choi, Y.-W., AlRukaibi, D., Eltahir, E. A. B.: Extreme storms in Southwest Asia (Northern Arabian Peninsula) under current and future climate, Clim. Dyn., 58, 1509-1524, https://link.springer.com/article/10.1007/s00382-021-05975-7, 2022.

Tyrlis, E., Lelieveld, J., and Steil, B.: The summer circulation over the eastern Mediterranean and the Middle East: Influence of the South Asian monsoon, Clim. Dyn., 40, 1103–1123, https://doi.org/10.1007/s00382-012-1528-4, 2013.

Waha, K., Krummenauer, L., Adams, S., Aich, V., Baarsch, F., Coumou, D., Fader, M., Hoff, H., Jobbins, G., Marcus, R., and Mengel, M.: Climate change impacts in the Middle East and northern Africa (MENA) region and their implications for vulnerable population groups, Reg. Environ. Change, 17, 1623–1638, https://doi.org/10.1007/s10113-017-1144-2, 2017.

Wang, T. and Li, T.: Factors controlling the diversities of MJO propagation and intensity, J. Climate, 34, 6549-6563, https://doi.org/10.1175/JCLI-D-20-0859.1, 2021.

Wei, Y. and Ren, H.-L.: Modulation of ENSO on Fast and Slow MJO Modes during Boreal Winter, J. Climate, 32, 7483–7506, https://doi.org/10.1175/JCLI-D-19-0013.1, 2019.

Wernli, H. and Sprenger, M.: Identification and ERA-15 climatology of potential vorticity streamers and cutoffs near the extratropical tropopause, J. Atmos. Sci., 64, 1569–1586, https://doi.org/10.1175/JAS3912.1, 2007.

Wheeler, M. C. and Hendon, H. H.: An All-Season Real-Time Multivariate MJO Index: Development of an Index for Monitoring and Prediction, Mon. Weather Rev., 132, 1917–1932, https://doi.org/10.1175/1520-0493(2004)132<1917:AARMMI>2.0.CO;2, 2004.

Wirth, V., Riemer, M., Chang, E. K. M., and Martius O.: Rossby wave packets on the midlatitude waveguide – a review. *Mon. Weath. Rev.* **146**, 1965-2001, 2018.

Zhang, C.: Madden–Julian oscillation: Bridging weather and climate. *Bull. Amer. Meteor. Soc.*, **94**, 1849–1870, https://doi.org/10.1175/BAMS-D-12-00026.1., 2013.

Zhou, Y., Kim, H., and Waliser, D. E.: Atmospheric River Lifecycle Responses to the Madden-Julian Oscillation, Geophys. Res. Lett., 48, 1–10, https://doi.org/10.1029/2020GL090983, 2021.

Zittis, G. Bruggeman, A. and Lelieveld, J.: Revisiting future extreme precipitation trends in the Mediterranean, Weath. Clim. Extremes, 34, 100380, https://doi.org/10.1016/j.wace.2021.100380, 2021.

Zittis, G., Almazroui, M., Alpert, P., Ciais, P., Cramer, W., Dahdal, Y., Fnais, M., Francis, D., Hadjinicolaou, P., Howari, F., Jrrar, A., Kaskaoutis, D. G., Kulmala, M., Lazoglou, G., Mihalopoulos, N., Lin, X., Rudich, Y., Sciare, J., Stenchikov, G., Xoplaki, E., and Lelieveld, J.: Climate Change and Weather Extremes in the Eastern Mediterranean and Middle East, Rev. Geophys., 60, e2021RG000762, https://doi.org/10.1029/2021RG000762, 2022.